4-28-2008

Measurement of correlated $b\bar{b}$ production in $p\bar{p}$ collisions at $s=1960$GeV

T. Aaltonen
Helsingin Yliopisto

A. Abulencia
University of Illinois Urbana-Champaign

J. Adelman
The Enrico Fermi Institute

T. Affolder
University of California, Santa Barbara

T. Akimoto
University of Tsukuba

See next page for additional authors

Recommended Citation

Aaltonen, T., Abulencia, A., Adelman, J., Affolder, T., Akimoto, T., Albrow, M., Amerio, S., Amidei, D., Anastassov, A., Anikeev, K., Annovi, A., Antos, J., Aoki, M., Apollinari, G., Arisawa, T., Artikov, A., Ashmanskas, W., Attal, A., Aurisano, A., Azfar, F., Azzi-Bacchetta, P., Azzurri, P., Bacchetta, N., Badgett, W., Barbaro-Galtieri, A., Barnes, V., Barnett, B., & Baroiant, S. (2008). Measurement of correlated $b\bar{b}$ production in $p\bar{p}$ collisions at $s=1960$GeV. *Physical Review D - Particles, Fields, Gravitation and Cosmology, 77* (7) https://doi.org/10.1103/PhysRevD.77.072004

Physics

Physics Research Publications

Purdue University *Year* 2008

Measurement of correlated b(b)over-bar production in p(p)over-bar collisions at root s=1960 GeV

T. Aaltonen, A. Abulencia, J. Adelman, T. Affolder, T. Akimoto, M. G. Albrow, S. Amerio, D. Amidei, A. Anastassov, K. Anikeev, A. Annovi, J. Antos, M. Aoki, G. Apollinari, T. Arisawa, A. Artikov, W. Ashmanskas, A. Attal, A. Aurisano, F. Azfar, P. Azzi-Bacchetta, P. Azzurri, N. Bacchetta, W. Badgett, A. Barbaro-Galtieri, V. E. Barnes, B. A. Barnett, S. Baroiant, V. Bartsch, G. Bauer, F. Bedeschi, S. Behari, G. Bellettini, J. Bellinger, A. Belloni, D. Benjamin, A. Beretvas, J. Beringer, T. Berry, A. Bhatti, M. Binkley, D. Bisello, I. Bizjak, R. E. Blair, C. Blocker, B. Blumenfeld, A. Bocci, A. Bodek, V. Boisvert, G. Bolla, A. Bolshov, D. Bortoletto, J. Boudreau, A. Boveia, B. Brau, L. Brigliadori, C. Bromberg, E. Brubaker, J. Budagov, H. S. Budd, S. Budd, K. Burkett, G. Busetto, P. Bussey, K. L. Byrum, S. Cabrera, M. Campanelli, M. Campbell, F. Canelli, A. Canepa, S. Carrillo, D. Carlsmith, R. Carosi, B. Casal, M. Casarsa, A. Castro, P. Catastini, D. Cauz, M. Cavalli-Sforza, A. Cerri, L. Cerrito, S. H. Chang, Y. C. Chen, M. Chertok, G. Chiarelli, G. Chlachidze, F. Chlebana, I. Cho, K. Cho, D. Chokheli, J. P. Chou, G. Choudalakis, S. H. Chuang, K. Chung, W. H. Chung, Y. S. Chung, M. Cilijak, C. I. Ciobanu, M. A. Ciocci, A. Clark, D. Clark, M. Coca, G. Compostella, M. E. Convery, J. Conway, B. Cooper, K. Copic, M. Cordelli, G. Cortiana, F. Crescioli, C. C. Almenar, J. Cuevas, R. Culbertson, J. C. Cully, S. DaRonco, M. Datta, S. D'Auria, T. Davies, D. Dagenhart, P. de Barbaro, S. De Cecco, A. Deisher, G. De Lentdecker, G. De Lorenzo, M. Dell'Orso, F. D. Paoli, L. Demortier, J. Deng, M. Deninno, D. De Pedis, P. F. Derwent, G. P. Di Giovanni, C. Dionisi, B. Di Ruzza, J. R. Dittmann, M. D'Onofrio, C. Dorr, S. Donati, P. Dong, J. Donini, T. Dorigo, S. Dube, J. Efron, R. Erbacher, D. Errede, S. Errede, R. Eusebi, H. C. Fang, S. Farrington, I. Fedorko, W. T. Fedorko, R. G. Feild, M. Feindt, J. P. Fernandez, R. Field, G. Flanagan, R. Forrest, S. Forrester, M. Franklin, J. C. Freeman, I. Furic, M. Gallinaro, J. Galyardt, J. E. Garcia, F. Garberson, A. F. Garfinkel, C. Gay, H. Gerberich, D. Gerdes, S. Giagu, P. Giannetti, K. Gibson, J. L. Gimmell, C. Ginsburg, N. Giokaris, M. Giordani, P. Giromini, M. Giunta, G.

Giurgiu, V. Glagolev, D. Glenzinski, M. Gold, N. Goldschmidt, J. Goldstein, A. Golossanov, G. Gomez, G. Gomez-Ceballos, M. Goncharov, O. Gonzalez, I. Gorelov, A. T. Goshaw, K. Goulianos, A. Gresele, S. Grinstein, C. Grosso-Pilcher, R. C. Group, U. Grundler, J. G. da Costa, Z. Gunay-Unalan, C. Haber, K. Hahn, S. R. Hahn, E. Halkiadakis, A. Hamilton, B. Y. Han, J. Y. Han, R. Handler, F. Happacher, K. Hara, D. Hare, M. Hare, S. Harper, R. F. Harr, R. M. Harris, M. Hartz, K. Hatakeyama, J. Hauser, C. Hays, M. Heck, A. Heijboer, B. Heinemann, J. Heinrich, C. Henderson, M. Herndon, J. Heuser, D. Hidas, C. S. Hill, D. Hirschbuehl, A. Hocker, A. Holloway, S. Hou, M. Houlden, S. C. Hsu, B. T. Huffman, R. E. Hughes, U. Husemann, J. Huston, J. Incandela, G. Introzzi, M. Iori, A. Ivanov, B. Iyutin, E. James, D. Jang, B. Jayatilaka, D. Jeans, E. J. Jeon, S. Jindariani, W. Johnson, M. Jones, K. K. Joo, S. Y. Jun, J. E. Jung, T. R. Junk, T. Kamon, P. E. Karchin, Y. Kato, Y. Kemp, R. Kephart, U. Kerzel, V. Khotilovich, B. Kilminster, D. H. Kim, H. S. Kim, J. E. Kim, M. J. Kim, S. B. Kim, S. H. Kim, Y. K. Kim, N. Kimura, L. Kirsch, S. Klimenko, M. Klute, B. Knuteson, B. R. Ko, K. Kondo, D. J. Kong, J. Konigsberg, A. Korytov, A. V. Kotwal, A. C. Kraan, J. Kraus, M. Kreps, J. Kroll, N. Krumnack, M. Kruse, V. Krutelyov, T. Kubo, S. E. Kuhlmann, T. Kuhr, N. P. Kulkarni, Y. Kusakabe, S. Kwang, A. T. Laasanen, S. Lami, S. Lammel, M. Lancaster, R. L. Lander, K. Lannon, A. Lath, G. Latino, I. Lazzizzera, T. LeCompte, J. Lee, J. Lee, Y. J. Lee, S. W. Lee, R. Lefevre, N. Leonardo, S. Leone, S. Levy, J. D. Lewis, C. Lin, C. S. Lin, M. Lindgren, E. Lipeles, A. Lister, D. O. Litvintsev, T. Liu, N. S. Lockyer, A. Loginov, M. Loreti, R. S. Lu, D. Lucchesi, P. Lujan, P. Lukens, G. Lungu, L. Lyons, J. Lys, R. Lysak, E. Lytken, P. Mack, R. Madrak, K. Maeshima, K. Makhoul, T. Maki, P. Maksimovic, S. Malde, S. Malik, G. Manca, A. Manousakis, F. Margaroli, R. Marginean, C. Marino, C. P. Marino, A. Martin, M. Martin, V. Martin, M. Martinez, R. Martinez-Ballarin, T. Maruyama, P. Mastrandrea, T. Masubuchi, H. Matsunaga, M. E. Mattson, P. Mazzanti, K. S. McFarland, P. McIntyre, R. McNulty, A. Mehta, P. Mehtala, S. Menzemer, A. Menzione, P. Merkel, C. Mesropian, A. Messina, T. Miao, N. Miladinovic, J. Miles, R. Miller, C. Mills, M. Milnik, A. Mitra, G. Mitselmakher, A. Miyamoto, S. Moed, N. Moggi, B. Mohr, C. S. Moon, R. Moore, M. Morello, P. M. Fernandez, J. Mulmenstadt, A. Mukherjee, T. Muller, R. Mumford, P. Murat, M. Mussini, J. Nachtman, A. Nagano, J. Naganoma, K. Nakamura, I. Nakano, A. Napier, V. Necula, C. Neu, M. S. Neubauer, J. Nielsen, L. Nodulman, O. Norniella, E. Nurse, S. H. Oh, Y. D. Oh, I. Oksuzian, T. Okusawa, R. Oldeman, R. Orava, K. Osterberg, C. Pagliarone, E. Palencia, V. Papadimitriou, A. Papaikonomou, A. A. Paramonov, B. Parks, J. Patrick, G. Pauletta, M. Paulini, C. Paus, D. E. Pellett, A. Penzo, T. J. Phillips, G. Piacentino, J. Piedra, L. Pinera, K. Pitts, C. Plager, L. Pondrom, X. Portell, O. Poukhov, N. Pounder, F. Prakoshyn, A. Pronko, J. Proudfoot, F. Ptohos, G. Punzi, J. Pursley, J. Rademacker, A. Rahaman, V. Ramakrishnan, N. Ranjan, I. Redondo, B. Reisert, V. Rekovic, P. Renton, M. Rescigno, S. Richter, F. Rimondi, L. Ristori, A. Robson, T. Rodrigo, E. Rogers, S. Rolli, R. Roser, M. Rossi, R. Rossin, A. Ruiz, J. Russ, V. Rusu, H. Saarikko, A. Safonov, W. K. Sakumoto, G. Salamanna, O. Salto, L. Santi, S. Sarkar, L. Sartori, K. Sato,

A. Savoy-Navarro, T. Scheidle, P. Schlabach, E. E. Schmidt, M. P. Schmidt, M. Schmitt, T. Schwarz, L. Scodellaro, A. L. Scott, A. Scribano, F. Scuri, A. Sedov, S. Seidel, Y. Seiya, A. Semenov, L. Sexton-Kennedy, A. Sfyrla, S. Z. Shalhout, M. D. Shapiro, T. Shears, P. F. Shepard, D. Sherman, M. Shimojima, M. Shochet, Y. Shon, I. Shreyber, A. Sidoti, A. Sisakyan, A. J. Slaughter, J. Slaunwhite, K. Sliwa, J. R. Smith, F. D. Snider, M. Soderberg, A. Soha, S. Somalwar, V. Sorin, J. Spalding, F. Spinella, P. Squillacioti, M. Stanitzki, A. Staveris-Polykalas, R. S. Denis, B. Stelzer, O. Stelzer-Chilton, D. Stentz, J. Strologas, D. Stuart, J. S. Suh, A. Sukhanov, H. Sun, I. Suslov, T. Suzuki, A. Taffard, R. Takashima, Y. Takeuchi, R. Tanaka, M. Tecchio, P. K. Teng, K. Terashi, J. Thom, A. S. Thompson, E. Thomson, P. Tipton, V. Tiwari, S. Tkaczyk, D. Toback, S. Tokar, K. Tollefson, T. Tomura, D. Tonelli, S. Torre, D. Torretta, S. Tourneur, S. Tsuno, Y. Tu, N. Turini, F. Ukegawa, S. Uozumi, S. Vallecorsa, N. van Remortel, A. Varganov, E. Vataga, F. Vazquez, G. Velev, C. Vellidis, G. Veramendi, V. Veszpremi, M. Vidal, R. Vidal, I. Vila, R. Vilar, T. Vine, M. Vogel, I. Volobouev, G. Volpi, F. Wurthwein, P. Wagner, R. G. Wagner, R. L. Wagner, J. Wagner, W. Wagner, R. Wallny, S. M. Wang, D. Waters, M. Weinberger, W. C. Wester, B. Whitehouse, D. Whiteson, E. Wicklund, H. H. Williams, P. Wilson, B. L. Winer, P. Wittich, S. Wolbers, C. Wolfe, T. Wright, X. Wu, S. M. Wynne, A. Yagil, K. Yamamoto, J. Yamaoka, T. Yamashita, C. Yang, U. K. Yang, Y. C. Yang, W. M. Yao, G. P. Yeh, J. Yoh, K. Yorita, T. Yoshida, G. B. Yu, I. Yu, S. S. Yu, J. C. Yun, L. Zanello, A. Zanetti, I. Zaw, X. Zhang, J. Zhou, and S. Zucchelli

Measurement of correlated $b\bar{b}$ production in $p\bar{p}$ collisions at $\sqrt{s} = 1960$ GeV

T. Aaltonen,[23] A. Abulencia,[24] J. Adelman,[13] T. Affolder,[10] T. Akimoto,[54] M. G. Albrow,[17] S. Amerio,[42] D. Amidei,[34] A. Anastassov,[51] K. Anikeev,[17] A. Annovi,[19] J. Antos,[14] M. Aoki,[54] G. Apollinari,[17] T. Arisawa,[56] A. Artikov,[15] W. Ashmanskas,[17] A. Attal,[3] A. Aurisano,[52] F. Azfar,[41] P. Azzi-Bacchetta,[42] P. Azzurri,[45] N. Bacchetta,[42] W. Badgett,[17] A. Barbaro-Galtieri,[29] V. E. Barnes,[47] B. A. Barnett,[25] S. Baroiant,[7] V. Bartsch,[31] G. Bauer,[33] F. Bedeschi,[45] S. Behari,[25] G. Bellettini,[45] J. Bellinger,[58] A. Belloni,[33] D. Benjamin,[16] A. Beretvas,[17] J. Beringer,[29] T. Berry,[30] A. Bhatti,[49] M. Binkley,[17] D. Bisello,[42] I. Bizjak,[31] R. E. Blair,[2] C. Blocker,[6] B. Blumenfeld,[25] A. Bocci,[16] A. Bodek,[48] V. Boisvert,[48] G. Bolla,[47] A. Bolshov,[33] D. Bortoletto,[47] J. Boudreau,[46] A. Boveia,[10] B. Brau,[10] L. Brigliadori,[5] C. Bromberg,[35] E. Brubaker,[13] J. Budagov,[15] H. S. Budd,[48] S. Budd,[24] K. Burkett,[17] G. Busetto,[42] P. Bussey,[21] K. L. Byrum,[2] S. Cabrera,[16,r] M. Campanelli,[20] M. Campbell,[34] F. Canelli,[17] A. Canepa,[44] S. Carrillo,[18,j] D. Carlsmith,[58] R. Carosi,[45] B. Casal,[11] M. Casarsa,[53] A. Castro,[5] P. Catastini,[45] D. Cauz,[53] M. Cavalli-Sforza,[3] A. Cerri,[29] L. Cerrito,[31,n] S. H. Chang,[28] Y. C. Chen,[1] M. Chertok,[7] G. Chiarelli,[45] G. Chlachidze,[17] F. Chlebana,[17] I. Cho,[28] K. Cho,[28] D. Chokheli,[15] J. P. Chou,[22] G. Choudalakis,[33] S. H. Chuang,[51] K. Chung,[12] W. H. Chung,[58] Y. S. Chung,[48] M. Cilijak,[45] C. I. Ciobanu,[24] M. A. Ciocci,[45] A. Clark,[20] D. Clark,[6] M. Coca,[16] G. Compostella,[42] M. E. Convery,[49] J. Conway,[7] B. Cooper,[31] K. Copic,[34] M. Cordelli,[19] G. Cortiana,[42] F. Crescioli,[45] C. Cuenca Almenar,[7,r] J. Cuevas,[11,m] R. Culbertson,[17] J. C. Cully,[34] S. DaRonco,[42] M. Datta,[17] S. D'Auria,[21] T. Davies,[21] D. Dagenhart,[17] P. de Barbaro,[48] S. De Cecco,[50] A. Deisher,[29] G. De Lentdecker,[48,d] G. De Lorenzo,[3] M. Dell'Orso,[45] F. Delli Paoli,[42] L. Demortier,[49] J. Deng,[16] M. Deninno,[5] D. De Pedis,[50] P. F. Derwent,[17] G. P. Di Giovanni,[43] C. Dionisi,[50] B. Di Ruzza,[53] J. R. Dittmann,[4] M. D'Onofrio,[3] C. Dörr,[26] S. Donati,[45] P. Dong,[8] J. Donini,[42] T. Dorigo,[42] S. Dube,[51] J. Efron,[38] R. Erbacher,[7] D. Errede,[24] S. Errede,[24] R. Eusebi,[17] H. C. Fang,[29] S. Farrington,[30] I. Fedorko,[45] W. T. Fedorko,[13] R. G. Feild,[59] M. Feindt,[26] J. P. Fernandez,[32] R. Field,[18] G. Flanagan,[47] R. Forrest,[7] S. Forrester,[7] M. Franklin,[22] J. C. Freeman,[29] I. Furic,[13] M. Gallinaro,[49] J. Galyardt,[12] J. E. Garcia,[45] F. Garberson,[10] A. F. Garfinkel,[47] C. Gay,[59] H. Gerberich,[24] D. Gerdes,[34] S. Giagu,[50] P. Giannetti,[45] K. Gibson,[46] J. L. Gimmell,[48] C. Ginsburg,[17] N. Giokaris,[15,b] M. Giordani,[53] P. Giromini,[19] M. Giunta,[45] G. Giurgiu,[25] V. Glagolev,[15] D. Glenzinski,[17] M. Gold,[36] N. Goldschmidt,[18] J. Goldstein,[41,c] A. Golossanov,[17] G. Gomez,[11] G. Gomez-Ceballos,[33] M. Goncharov,[52] O. González,[32] I. Gorelov,[36] A. T. Goshaw,[16] K. Goulianos,[49] A. Gresele,[42] S. Grinstein,[22] C. Grosso-Pilcher,[13] R. C. Group,[17] U. Grundler,[24] J. Guimaraes da Costa,[22] Z. Gunay-Unalan,[35] C. Haber,[29] K. Hahn,[33] S. R. Hahn,[17] E. Halkiadakis,[51] A. Hamilton,[20] B.-Y. Han,[48] J. Y. Han,[48] R. Handler,[58] F. Happacher,[19] K. Hara,[54] D. Hare,[51] M. Hare,[55] S. Harper,[41] R. F. Harr,[57] R. M. Harris,[17] M. Hartz,[46] K. Hatakeyama,[49] J. Hauser,[8] C. Hays,[41] M. Heck,[26] A. Heijboer,[44] B. Heinemann,[29] J. Heinrich,[44] C. Henderson,[33] M. Herndon,[58] J. Heuser,[26] D. Hidas,[16] C. S. Hill,[10,c] D. Hirschbuehl,[26] A. Hocker,[17] A. Holloway,[22] S. Hou,[1] M. Houlden,[30] S.-C. Hsu,[9] B. T. Huffman,[41] R. E. Hughes,[38] U. Husemann,[59] J. Huston,[35] J. Incandela,[10] G. Introzzi,[45] M. Iori,[50] A. Ivanov,[7] B. Iyutin,[33] E. James,[17] D. Jang,[51] B. Jayatilaka,[16] D. Jeans,[50] E. J. Jeon,[28] S. Jindariani,[18] W. Johnson,[7] M. Jones,[47] K. K. Joo,[28] S. Y. Jun,[12] J. E. Jung,[28] T. R. Junk,[24] T. Kamon,[52] P. E. Karchin,[57] Y. Kato,[40] Y. Kemp,[26] R. Kephart,[17] U. Kerzel,[26] V. Khotilovich,[52] B. Kilminster,[38] D. H. Kim,[28] H. S. Kim,[28] J. E. Kim,[28] M. J. Kim,[17] S. B. Kim,[28] S. H. Kim,[54] Y. K. Kim,[13] N. Kimura,[54] L. Kirsch,[6] S. Klimenko,[18] M. Klute,[33] B. Knuteson,[33] B. R. Ko,[16] K. Kondo,[56] D. J. Kong,[28] J. Konigsberg,[18] A. Korytov,[18] A. V. Kotwal,[16] A. C. Kraan,[44] J. Kraus,[24] M. Kreps,[26] J. Kroll,[44] N. Krumnack,[4] M. Kruse,[16] V. Krutelyov,[10] T. Kubo,[54] S. E. Kuhlmann,[2] T. Kuhr,[26] N. P. Kulkarni,[57] Y. Kusakabe,[56] S. Kwang,[13] A. T. Laasanen,[47] S. Lami,[45] S. Lammel,[17] M. Lancaster,[31] R. L. Lander,[7] K. Lannon,[38] A. Lath,[51] G. Latino,[45] I. Lazzizzera,[42] T. LeCompte,[2] J. Lee,[48] J. Lee,[28] Y. J. Lee,[28] S. W. Lee,[52,p] R. Lefèvre,[20] N. Leonardo,[33] S. Leone,[45] S. Levy,[13] J. D. Lewis,[17] C. Lin,[59] C. S. Lin,[17] M. Lindgren,[17] E. Lipeles,[9] A. Lister,[7] D. O. Litvintsev,[17] T. Liu,[17] N. S. Lockyer,[44] A. Loginov,[59] M. Loreti,[42] R.-S. Lu,[1] D. Lucchesi,[42] P. Lujan,[29] P. Lukens,[17] G. Lungu,[18] L. Lyons,[41] J. Lys,[29] R. Lysak,[14] E. Lytken,[47] P. Mack,[26] R. Madrak,[17] K. Maeshima,[17] K. Makhoul,[33] T. Maki,[23] P. Maksimovic,[25] S. Malde,[41] S. Malik,[31] G. Manca,[30] A. Manousakis,[15,b] F. Margaroli,[5] R. Marginean,[17] C. Marino,[26] C. P. Marino,[24] A. Martin,[59] M. Martin,[25] V. Martin,[21,h] M. Martínez,[3] R. Martínez-Ballarín,[32] T. Maruyama,[54] P. Mastrandrea,[50] T. Masubuchi,[54] H. Matsunaga,[54] M. E. Mattson,[57] P. Mazzanti,[5] K. S. McFarland,[48] P. McIntyre,[52] R. McNulty,[30,g] A. Mehta,[30] P. Mehtala,[23] S. Menzemer,[11,i] A. Menzione,[45] P. Merkel,[47] C. Mesropian,[49] A. Messina,[35] T. Miao,[17] N. Miladinovic,[6] J. Miles,[33] R. Miller,[35] C. Mills,[10] M. Milnik,[26] A. Mitra,[1] G. Mitselmakher,[18] A. Miyamoto,[27] S. Moed,[20] N. Moggi,[5] B. Mohr,[8] C. S. Moon,[28] R. Moore,[17] M. Morello,[45] P. Movilla Fernandez,[29] J. Mülmenstädt,[29] A. Mukherjee,[17] Th. Muller,[26] R. Mumford,[25] P. Murat,[17] M. Mussini,[5] J. Nachtman,[17] A. Nagano,[54] J. Naganoma,[56] K. Nakamura,[54] I. Nakano,[39] A. Napier,[55] V. Necula,[16] C. Neu,[44] M. S. Neubauer,[9] J. Nielsen,[29,o]

L. Nodulman,[2] O. Norniella,[3] E. Nurse,[31] S. H. Oh,[16] Y. D. Oh,[28] I. Oksuzian,[18] T. Okusawa,[40] R. Oldeman,[30] R. Orava,[23] K. Osterberg,[23] C. Pagliarone,[45] E. Palencia,[11] V. Papadimitriou,[17] A. Papaikonomou,[26] A. A. Paramonov,[13] B. Parks,[38] J. Patrick,[17] G. Pauletta,[53] M. Paulini,[12] C. Paus,[33] D. E. Pellett,[7] A. Penzo,[53] T. J. Phillips,[16] G. Piacentino,[45] J. Piedra,[43] L. Pinera,[18] K. Pitts,[24] C. Plager,[8] L. Pondrom,[58] X. Portell,[3] O. Poukhov,[15] N. Pounder,[41] F. Prakoshyn,[15] A. Pronko,[17] J. Proudfoot,[2] F. Ptohos,[19,f] G. Punzi,[45] J. Pursley,[25] J. Rademacker,[41,c] A. Rahaman,[46] V. Ramakrishnan,[58] N. Ranjan,[47] I. Redondo,[32] B. Reisert,[17] V. Rekovic,[36] P. Renton,[41] M. Rescigno,[50] S. Richter,[26] F. Rimondi,[5] L. Ristori,[45] A. Robson,[21] T. Rodrigo,[11] E. Rogers,[24] S. Rolli,[55] R. Roser,[17] M. Rossi,[53] R. Rossin,[10] A. Ruiz,[11] J. Russ,[12] V. Rusu,[13] H. Saarikko,[23] A. Safonov,[52] W. K. Sakumoto,[48] G. Salamanna,[50] O. Saltó,[3] L. Santi,[53] S. Sarkar,[50] L. Sartori,[45] K. Sato,[17] A. Savoy-Navarro,[43] T. Scheidle,[26] P. Schlabach,[17] E. E. Schmidt,[17] M. P. Schmidt,[59] M. Schmitt,[37] T. Schwarz,[7] L. Scodellaro,[11] A. L. Scott,[10] A. Scribano,[45] F. Scuri,[45] A. Sedov,[47] S. Seidel,[36] Y. Seiya,[40] A. Semenov,[15] L. Sexton-Kennedy,[17] A. Sfyrla,[20] S. Z. Shalhout,[57] M. D. Shapiro,[29] T. Shears,[30] P. F. Shepard,[46] D. Sherman,[22] M. Shimojima,[54,l] M. Shochet,[13] Y. Shon,[58] I. Shreyber,[20] A. Sidoti,[45] A. Sisakyan,[15] A. J. Slaughter,[17] J. Slaunwhite,[38] K. Sliwa,[55] J. R. Smith,[7] F. D. Snider,[17] M. Soderberg,[34] A. Soha,[7] S. Somalwar,[51] V. Sorin,[35] J. Spalding,[17] F. Spinella,[45] P. Squillacioti,[45] M. Stanitzki,[59] A. Staveris-Polykalas,[45] R. St. Denis,[21] B. Stelzer,[8] O. Stelzer-Chilton,[41] D. Stentz,[37] J. Strologas,[36] D. Stuart,[10] J. S. Suh,[28] A. Sukhanov,[18] H. Sun,[55] I. Suslov,[15] T. Suzuki,[54] A. Taffard,[24,q] R. Takashima,[39] Y. Takeuchi,[54] R. Tanaka,[39] M. Tecchio,[34] P. K. Teng,[1] K. Terashi,[49] J. Thom,[17,e] A. S. Thompson,[21] E. Thomson,[44] P. Tipton,[59] V. Tiwari,[12] S. Tkaczyk,[17] D. Toback,[52] S. Tokar,[14] K. Tollefson,[35] T. Tomura,[54] D. Tonelli,[45] S. Torre,[19] D. Torretta,[17] S. Tourneur,[43] S. Tsuno,[39] Y. Tu,[44] N. Turini,[45] F. Ukegawa,[54] S. Uozumi,[54] S. Vallecorsa,[20] N. van Remortel,[23] A. Varganov,[34] E. Vataga,[36] F. Vazquez,[18,j] G. Velev,[17] C. Vellidis,[45,b] G. Veramendi,[24] V. Veszpremi,[47] M. Vidal,[32] R. Vidal,[17] I. Vila,[11] R. Vilar,[11] T. Vine,[31] M. Vogel,[36] I. Volobouev,[29,p] G. Volpi,[45] F. Würthwein,[9] P. Wagner,[52] R. G. Wagner,[2] R. L. Wagner,[17] J. Wagner,[26] W. Wagner,[26] R. Wallny,[8] S. M. Wang,[1] D. Waters,[31] M. Weinberger,[52] W. C. Wester III,[17] B. Whitehouse,[55] D. Whiteson,[44,q] E. Wicklund,[17] H. H. Williams,[44] P. Wilson,[17] B. L. Winer,[38] P. Wittich,[17,e] S. Wolbers,[17] C. Wolfe,[13] T. Wright,[34] X. Wu,[20] S. M. Wynne,[30] A. Yagil,[9] K. Yamamoto,[40] J. Yamaoka,[51] T. Yamashita,[39] C. Yang,[59] U. K. Yang,[13,k] Y. C. Yang,[28] W. M. Yao,[29] G. P. Yeh,[17] J. Yoh,[17] K. Yorita,[13] T. Yoshida,[40] G. B. Yu,[48] I. Yu,[28] S. S. Yu,[17] J. C. Yun,[17] L. Zanello,[50] A. Zanetti,[53] I. Zaw,[22] X. Zhang,[24] J. Zhou,[51] and S. Zucchelli[5]

(CDF Collaboration)[a]

[1]*Institute of Physics, Academia Sinica, Taipei, Taiwan 11529, Republic of China*
[2]*Argonne National Laboratory, Argonne, Illinois 60439, USA*
[3]*Institut de Fisica d'Altes Energies, Universitat Autonoma de Barcelona, E-08193, Bellaterra (Barcelona), Spain*
[4]*Baylor University, Waco, Texas 76798, USA*
[5]*Istituto Nazionale di Fisica Nucleare, University of Bologna, I-40127 Bologna, Italy*
[6]*Brandeis University, Waltham, Massachusetts 02254, USA*
[7]*University of California, Davis, Davis, California 95616, USA*
[8]*University of California, Los Angeles, Los Angeles, California 90024, USA*
[9]*University of California, San Diego, La Jolla, California 92093, USA*
[10]*University of California, Santa Barbara,, Santa Barbara, California 93106, USA*
[11]*Instituto de Fisica de Cantabria, CSIC-University of Cantabria, 39005 Santander, Spain*
[12]*Carnegie Mellon University, Pittsburgh, Pennsylvania 15213, USA*
[13]*Enrico Fermi Institute, University of Chicago, Chicago, Illinois 60637, USA*
[14]*Comenius University, 842 48 Bratislava, Slovakia;*
Institute of Experimental Physics, 040 01 Kosice, Slovakia
[15]*Joint Institute for Nuclear Research, RU-141980 Dubna, Russia*
[16]*Duke University, Durham, North Carolina 27708*
[17]*Fermi National Accelerator Laboratory, Batavia, Illinois 60510, USA*
[18]*University of Florida, Gainesville, Florida 32611, USA*
[19]*Laboratori Nazionali di Frascati, Istituto Nazionale di Fisica Nucleare, I-00044 Frascati, Italy*
[20]*University of Geneva, CH-1211 Geneva 4, Switzerland*
[21]*Glasgow University, Glasgow G12 8QQ, United Kingdom*
[22]*Harvard University, Cambridge, Massachusetts 02138, USA*
[23]*Division of High Energy Physics, Department of Physics, University of Helsinki*
and Helsinki Institute of Physics, FIN-00014, Helsinki, Finland
[24]*University of Illinois, Urbana, Illinois 61801, USA*
[25]*The Johns Hopkins University, Baltimore, Maryland 21218, USA*

[26]*Institut für Experimentelle Kernphysik, Universität Karlsruhe, 76128 Karlsruhe, Germany*
[27]*High Energy Accelerator Research Organization (KEK), Tsukuba, Ibaraki 305, Japan*
[28]*Center for High Energy Physics: Kyungpook National University, Taegu 702-701, Korea;*
Seoul National University, Seoul 151-742, Korea;
SungKyunKwan University, Suwon 440-746, Korea
[29]*Ernest Orlando Lawrence Berkeley National Laboratory, Berkeley, California 94720, USA*
[30]*University of Liverpool, Liverpool L69 7ZE, United Kingdom*
[31]*University College London, London WC1E 6BT, United Kingdom*
[32]*Centro de Investigaciones Energeticas, Medioambientales y Tecnologicas, E-28040 Madrid, Spain*
[33]*Massachusetts Institute of Technology, Cambridge, Massachusetts 02139, USA*
[34]*University of Michigan, Ann Arbor, Michigan 48109, USA*
[35]*Michigan State University, East Lansing, Michigan 48824, USA*
[36]*University of New Mexico, Albuquerque, New Mexico 87131, USA*
[37]*Northwestern University, Evanston, Illinois 60208, USA*
[38]*The Ohio State University, Columbus, Ohio 43210, USA*
[39]*Okayama University, Okayama 700-8530, Japan*
[40]*Osaka City University, Osaka 588, Japan*
[41]*University of Oxford, Oxford OX1 3RH, United Kingdom*
[42]*University of Padova, Istituto Nazionale di Fisica Nucleare, Sezione di Padova-Trento, I-35131 Padova, Italy*
[43]*LPNHE, Universite Pierre et Marie Curie/IN2P3-CNRS, UMR7585, Paris, F-75252 France*
[44]*University of Pennsylvania, Philadelphia, Pennsylvania 19104, USA*
[45]*Istituto Nazionale di Fisica Nucleare Pisa, Universities of Pisa, Siena*
and Scuola Normale Superiore, I-56127 Pisa, Italy
[46]*University of Pittsburgh, Pittsburgh, Pennsylvania 15260, USA*
[47]*Purdue University, West Lafayette, Indiana 47907, USA*
[48]*University of Rochester, Rochester, New York 14627, USA*
[49]*The Rockefeller University, New York, New York 10021, USA*
[50]*Istituto Nazionale di Fisica Nucleare, Sezione di Roma 1, University of Rome "La Sapienza," I-00185 Roma, Italy*
[51]*Rutgers University, Piscataway, New Jersey 08855, USA*
[52]*Texas A&M University, College Station, Texas 77843, USA*
[53]*Istituto Nazionale di Fisica Nucleare, University of Trieste/Udine, Italy*
[54]*University of Tsukuba, Tsukuba, Ibaraki 305, Japan*
[55]*Tufts University, Medford, Massachusetts 02155, USA*
[56]*Waseda University, Tokyo 169, Japan*
[57]*Wayne State University, Detroit, Michigan 48201, USA*
[58]*University of Wisconsin, Madison, Wisconsin 53706, USA*
[59]*Yale University, New Haven, Connecticut 06520, USA*
(Received 9 October 2007; published 28 April 2008)

We present a measurement of the correlated $b\bar{b}$ production cross section. The data used in this analysis were taken with the upgraded CDF detector (CDF II) at the Fermilab Tevatron collider, and correspond to an integrated luminosity of 742 pb^{-1}. We utilize muon pairs with invariant mass $5 \leq m_{\mu\mu} \leq 80$ GeV/c^2

[a]With visitors from
[b]University of Athens, 15784 Athens, Greece.
[c]University of Bristol, Bristol BS8 1TL, United Kingdom.
[d]University Libre de Bruxelles, B-1050 Brussels, Belgium.
[e]Cornell University, Ithaca, NY 14853, USA.
[f]University of Cyprus, Nicosia CY-1678, Cyprus.
[g]University College Dublin, Dublin 4, Ireland.
[h]University of Edinburgh, Edinburgh EH9 3JZ, United Kingdom.
[i]University of Heidelberg, D-69120 Heidelberg, Germany.
[j]Universidad Iberoamericana, Mexico D. F., Mexico.
[k]University of Manchester, Manchester M13 9PL, United Kingdom.
[l]Nagasaki Institute of Applied Science, Nagasaki, Japan.
[m]University de Oviedo, E-33007 Oviedo, Spain.
[n]University of London, Queen Mary College, London, E1 4NS, United Kingdom.
[o]University of California, Santa Cruz, Santa Cruz, CA 95064, USA.
[p]Texas Tech University, Lubbock, TX 79409, USA.
[q]University of California, Irvine, Irvine, CA 92697, USA.
[r]IFIC (CSIC-Universitat de Valencia), 46071 Valencia, Spain.

produced by $b\bar{b}$ double semileptonic decays. For muons with $p_T \geq 3$ GeV/c and $|\eta| \leq 0.7$, that are produced by b and $\bar{b}$ quarks with $p_T \geq 2$ GeV/c and $|y| \leq 1.3$, we measure $\sigma_{b\to\mu,\bar{b}\to\mu} = 1549 \pm 133$ pb. We compare this result with theoretical predictions and previous measurements. We also report the measurement of $\sigma_{c\to\mu,\bar{c}\to\mu}$, a by-product of the study of the background to $b\bar{b}$ production.

DOI: 10.1103/PhysRevD.77.072004 PACS numbers: 14.65.Fy, 12.38.Qk, 13.85.Qk, 14.65.Dw

I. INTRODUCTION

Measurements of the cross section for producing, in hadronic collisions, both b and $\bar{b}$ quarks centrally and above a given transverse momentum threshold (typically $p_T \geq 5$–20 GeV/c), referred to as $\sigma_{b\bar{b}}$ or $b\bar{b}$ correlations, provide an important test of the predictive power of quantum chromodynamics (QCD). Experimentally, $b\bar{b}$ correlations at the Tevatron are inferred from the production rate above a given p_T threshold of some of the decay products (leptons or tracks consistent with a secondary displaced vertex) of both b and $\bar{b}$ hadrons. In QCD calculations, the long- and short-distance dynamics of the hadronic hard-scattering cross section are factorized into nonperturbative parton distribution functions (PDF) and fragmentation functions, and perturbatively calculable hard-scattering functions. At the perturbative level, the hard-scattering function can be evaluated at leading-order (LO) and next-to-leading order (NLO) with the MNR Monte Carlo program [1]. In contrast with the exact NLO prediction of the single b quark production cross section,[1] the exact NLO calculation of $\sigma_{b\bar{b}}$ appears to be a robust perturbative QCD prediction. As noted in Ref. [5], the exact LO and NLO prediction of $\sigma_{b\bar{b}}$ are equal within a few percent, and the NLO result does not change by more than 15% when varying the renormalization and factorization scales by a factor of 2 and the b quark pole mass ($m_b = 4.75$ GeV/c^2) by 0.25 GeV/c^2. The exact NLO prediction of $\sigma_{b\bar{b}}$ is quite insensitive to the choice of PDF fits when they include HERA data and yield a value of the QCD coupling strength consistent with LEP data ($\alpha_s(m_Z) \simeq 0.118$) [6–8]. However, when comparing to the data, the apparent robustness of the $\sigma_{b\bar{b}}$ calculation could be spoiled by the inclusion of nonperturbative fragmentation functions that connect b-quark and b-hadron distributions. Traditionally, data to theory comparisons use a fragmentation model based on the Peterson function [9] with the ϵ parameter set to 0.006 according to fits to e^+e^- data [10]. However, as noted in Ref. [11], the Peterson fragmentation function has been tuned to the data in conjunction with LO parton-level cross sections evaluated with parton-shower event generators, and cannot be consistently convoluted with the exact NLO calculation. As an example, the FONLL calculation [12] implements the exact NLO prediction of the single b-quark cross section with the resummation of (p_T/m_b) logarithms with next-to-leading accuracy (NLL). A calculation with the same level of accuracy, available for the production of b quarks at e^+e^- colliders [13], has been used to extract consistent nonperturbative fragmentation functions from LEP and SLC data [14]. These fragmentation functions appear to be harder than the Peterson fragmentation [11]. Unfortunately, they also cannot be consistently convoluted with the exact NLO calculation of $\sigma_{b\bar{b}}$ for which NLL logarithmic corrections have yet to be evaluated.

Alternatively, the production of pairs of b and $\bar{b}$ hadrons can be estimated with event generators that are based on the LO calculation combined with a leading-logarithmic (LL) treatment of higher orders via the parton-shower approximation, such as the HERWIG [15] and PYTHIA [16] Monte Carlo programs. The MC@NLO event generator [17] merges the exact NLO matrix element with the LL shower evolution and hadronization performed by the HERWIG parton-shower Monte Carlo. In some cases, event generators that combine exact LO or NLO calculations with LL parton-shower simulations return parton-level cross sections that are quite different from the exact NLO calculation [1]. The MC@NLO method suffers the additional problem that the HERWIG model of the b quark hadronization has been tuned to e^+e^- data using LO parton-level cross sections. The benefits and pitfalls of each theoretical approach are discussed in more detail in Refs. [17–19].

Precise measurements of the pair production of b and $\bar{b}$ hadrons at the Tevatron could contribute to improve the modeling of fragmentation functions consistent with the exact NLO calculation. Unfortunately, as noted in Ref. [6], the status of the $\sigma_{b\bar{b}}$ measurements at the Tevatron is quite disconcerting. Five measurements of $\sigma_{b\bar{b}}$ have been performed by the CDF and D0 collaborations. Reference [6] compares the results of different experiments using R_{2b}, the ratio of the measured $\sigma_{b\bar{b}}$ to the exact NLO prediction (the b-quark and b-hadron distributions are connected via the LL HERWIG fragmentation model or the Peterson fragmentation function).

The study in Ref. [5] (CDF) uses two central jets with $E_T \geq 15$ GeV, each containing a secondary vertex due to b- or $\bar{b}$-quark decays. The measurement yields $R_{2b} = 1.2 \pm 0.3$.

The study in Ref. [20] (CDF) uses events containing two central jets with $E_T \geq 30$ and 20 GeV, respectively; pairs

[1]The single b quark cross section can be evaluated at exact NLO accuracy with the NDE Monte Carlo generator [2]. The calculation is affected by an uncertainty as large as 50% due to the choice of renormalization and factorization scales and by additional, but smaller, uncertainties due to choice of the PDF fits or the b-quark mass [3]. At perturbative level, the large scale dependence of the NLO calculation is interpreted as a symptom of large higher-order contributions [4].

of b jets are also identified by requiring the presence of displaced secondary vertices. This study yields[2] $R_{2b} = 1.1 \pm 0.3$.

The study in Ref. [21] (CDF) uses events containing muons from b-quark semileptonic decays that recoil against a jet that contains tracks with large impact parameter (b jet). This study yields $R_{2b} = 1.5 \pm 0.2$ for b and $\bar{b}$ quarks produced centrally with $p_T \geq 12$ GeV/c.

References [22] (CDF) and [23] (D0) report measurements that use two central muons arising from b-quark semileptonic decays. The measurements yield $R_{2b} = 3.0 \pm 0.6$ and $R_{2b} = 2.3 \pm 0.7$ for central b and $\bar{b}$ quarks with $p_T \geq 6$ and 7 GeV/c, respectively.

The five measurements yield $\langle R_{2b} \rangle = 1.8$ with a 0.8 rms deviation [6]. Such a large rms deviation is a likely indication of experimental difficulties.[3] This type of discrepancy could result from an underestimate of the kinematic and detector acceptance for semileptonic b decays or of the underlying background. However, measurements of the single b-quark production cross section based upon detection of semileptonic b-quark decays suggest otherwise because they are approximately 35% smaller than those based on detection of J/ψ mesons from b-quark decays [6,24]. The present discrepancy could also be explained by postulating the production of additional objects with a 100% semileptonic branching ratio and a cross section of the order of $1/10$ of the b cross section as investigated in Ref. [5]. Therefore, it is of interest to clarify the experimental situation. This paper reports a new measurement of $\sigma_{b\bar{b}}$ that uses dimuons arising from $b\bar{b}$ production. At the Tevatron, dimuon events result from decays of heavy quark pairs ($b\bar{b}$ and $c\bar{c}$), the Drell-Yan process, charmonium and bottomonium decays, and decays of π and K mesons. Background to dimuon events also comes from the misidentification of π or K mesons. As in previous studies [22,25], we make use of the precision tracking provided by the CDF silicon microvertex detector to evaluate the fractions of muons due to long-lived b- and c-hadron decays, and to the other background contributions.

Sections II and III describe the detector systems relevant to this analysis and the data selection, respectively. The analysis method is discussed in Sec. IV, while the heavy flavor composition of the dimuon sample is determined in Sec. V. The kinematic and detector acceptance is evaluated in Sec. VI. The dimuon cross section is derived and compared to theoretical expectation and previous measurements in Sec. VII. Our conclusions are summarized in Sec. VIII.

[2]Ref. [20] compares the data to the MC@NLO prediction, which is 12% smaller than the exact NLO prediction. This difference was not appreciated in Ref. [6].

[3]This includes the possibility that in some cases the NLO prediction has been evaluated incorrectly.

II. CDF II DETECTOR AND TRIGGER

CDF II is a multipurpose detector, equipped with a charged particle spectrometer and a finely segmented calorimeter. In this section, we describe the detector components that are relevant to this analysis. The description of these subsystems can be found in Refs. [26–35]. Two devices inside the 1.4 T solenoid are used for measuring the momentum of charged particles: the silicon vertex detector (SVXII and ISL) and the central tracking chamber (COT). The SVXII detector consists of microstrip sensors arranged in six cylindrical shells with radii between 1.5 and 10.6 cm, and with a total z coverage[4] of 90 cm. The first SVXII layer, also referred to as L00 detector, is made of single-sided sensors mounted on the beryllium beam pipe. The remaining five SVXII layers are made of double-sided sensors and are divided into three contiguous five-layer sections along the beam direction z. The vertex z-distribution for $p\bar{p}$ collisions is approximately described by a Gaussian function with a sigma of 28 cm. The transverse profile of the Tevatron beam is circular and has an rms spread of $\simeq 25$ μm in the horizontal and vertical directions. The SVXII single-hit resolution is approximately 11 μm and allows a track impact parameter[5] resolution of approximately 35 μm, when also including the effect of the beam transverse size. The two additional silicon layers of the ISL help to link tracks in the COT to hits in the SVXII. The COT is a cylindrical drift chamber containing 96 sense wire layers grouped into eight alternating superlayers of axial and stereo wires. Its active volume covers $|z| \leq 155$ cm and 40 to 140 cm in radius. The transverse momentum resolution of tracks reconstructed using COT hits is $\sigma(p_T)/p_T^2 \simeq 0.0017$ [GeV/c]$^{-1}$. COT tracks are extrapolated into the SVXII detector and refitted adding hits consistent with the track extrapolation.

The central muon detector (CMU) is located around the central electromagnetic and hadronic calorimeters, which have a thickness of 5.5 interaction lengths at normal incidence. The CMU detector covers a nominal pseudorapidity range $|\eta| \leq 0.63$ relative to the center of the detector, and is segmented into two barrels of 24 modules, each covering 15° in ϕ. Every module is further segmented into three submodules, each covering 4.2° in ϕ and consisting of four layers of drift chambers. The smallest drift unit, called a stack, covers a 1.2° angle in ϕ. Adjacent pairs of stacks are combined together into a tower. A track segment (hits in

[4]In the CDF coordinate system, θ and ϕ are the polar and azimuthal angles of a track, respectively, defined with respect to the proton beam direction, z. The pseudorapidity η is defined as $-\log\tan(\theta/2)$. The transverse momentum of a particle is $p_T = p\sin(\theta)$. The rapidity is defined as $y = 1/2 \cdot \log((E + p_z)/(E - p_z))$, where E and p_z are the energy and longitudinal momentum of the particle associated with the track.

[5]The impact parameter d is the distance of closest approach of a track to the primary event vertex in the transverse plane.

two out of four layers of a stack) detected in a tower is referred to as a CMU stub. A second set of muon drift chambers (CMP) is located behind an additional steel absorber of 3.3 interaction lengths. The chambers are 640 cm long and are arranged axially to form a box around the central detector. The CMP detector covers a nominal pseudorapidity range $|\eta| \leq 0.54$ relative to the center of the detector. Muons which produce a stub in both CMU and CMP systems are called CMUP muons.

The luminosity is measured using gaseous Cherenkov counters that monitor the rate of inelastic $p\bar{p}$ collisions. The inelastic $p\bar{p}$ cross section at $\sqrt{s} = 1960$ GeV is scaled from measurements at $\sqrt{s} = 1800$ GeV using the calculations in Ref. [36]. The integrated luminosity is determined with a 6% systematic uncertainty [37].

CDF uses a three-level trigger system. At Level 1 (L1), data from every beam crossing are stored in a pipeline capable of buffering data from 42 beam crossings. The L1 trigger either rejects events or copies them into one of the four Level 2 (L2) buffers. Events that pass the L1 and L2 selection criteria are sent to the Level 3 (L3) trigger, a cluster of computers running speed-optimized reconstruction code.

For this study, we select events with two muon candidates identified by the L1 and L2 triggers. The L1 trigger uses tracks with $p_T \geq 1.5$ GeV/c found by a fast track processor (XFT). The XFT examines COT hits from the four axial superlayers and provides $r - \phi$ information. The XFT finds tracks with $p_T \geq 1.5$ GeV/c in azimuthal sections of 1.25°. The XFT passes the tracks to a set of extrapolation units that determine the CMU towers in which a CMU stub should be found if the track is a muon. If a stub is found, a L1 CMU primitive is generated. The L1 dimuon trigger requires at least two CMU primitives, separated by at least two CMU towers. The L2 trigger additionally requires that at least one of the muons has a CMUP stub matched to an XFT track with $p_T \geq 3$ GeV/c. All these trigger requirements are emulated by the detector simulation on a run-by-run basis. The L3 trigger requires a pair of CMUP muons with invariant mass larger than 5 GeV/c^2, and $|\delta z_0| \leq 5$ cm, where z_0 is the z coordinate of the muon track at its point of closest approach to the beam line in the $r - \phi$ plane. These requirements define the dimuon trigger used in this analysis.

We use additional triggers in order to measure detection efficiencies and verify the detector simulation. The first trigger (CMUP$_{p_T}$4) selects events with at least one CMUP primitive with $p_T \geq 4$ GeV/c identified by both the L1 and L2 triggers, and an additional muon found by the L3 algorithms. Events collected with this trigger are used to measure the muon trigger efficiency. The second trigger requires a L1 CMUP primitive with $p_T \geq 4$ GeV/c accompanied by a L2 requirement of an additional track with $p_T \geq 2$ GeV/c and impact parameter $0.12 \leq d \leq 1$ mm as measured by the silicon vertex trigger (SVT) [38]. The SVT calculates the impact parameter of each XFT track, with respect to the beam line, with a 50 μm resolution that includes the 25 μm contribution of the beam transverse width. Events selected with this trigger (μ-SVT) are used to verify the muon detector acceptance and the muon reconstruction efficiency. The last trigger (CHARM) acquires events with two SVT tracks with $p_T \geq 2$ GeV/c and with impact parameter $0.12 \leq d \leq 1$ mm. In this data sample, we reconstruct $D^0 \rightarrow K\pi$ decays to measure the probability that a charged hadron mimics the signal of a CMUP muon. We also use $J/\psi \rightarrow \mu^+\mu^-$ events acquired with the J/ψ trigger. At L1 and L2, this trigger requires two CMU primitives corresponding to tracks with $p_T \geq 1.5$ GeV/c. At L3, muons are required to have opposite charges and an invariant mass in the window 2.7–4.0 GeV/c^2. These events are used to calibrate the efficiency of the SVXII detector and of stricter requirements used for selecting CMUP muons.

III. DATA SELECTION

In this analysis, we select events acquired with the dimuon trigger and which contain two and only two CMUP muons with same or opposite charge. Events are reconstructed offline taking advantage of more refined calibration constants and reconstruction algorithms. COT tracks are extrapolated into the SVXII detector, and refitted adding hits consistent with the track extrapolation. Stubs reconstructed in the CMU and CMP detectors are matched to tracks with $p_T \geq 3$ GeV/c. A track is identified as a CMUP muon if $\Delta r\phi$, the distance in the $r - \phi$ plane between the track projected to the CMU (CMP) chambers and a CMU (CMP) stub, is less than 20 (40) cm. We require that muon-candidate stubs correspond to a L1 CMU primitive, and correct the muon momentum for energy losses in the detector.

To ensure an accurate impact parameter measurement, each muon track is required to be reconstructed in the SVXII detector with hits in the two inner layers and in at least two of the remaining four external layers. We evaluate the impact parameter of each muon track with respect to the primary vertex. We reconstruct primary vertices using all tracks with SVXII hits that are consistent with originating from a common vertex. In events in which more than one interaction vertex has been reconstructed we use the one closest in z to the average of the muon track z_0-positions and within a 6 cm distance. The primary vertex coordinates transverse to the beam direction have rms uncertainties of approximately 3 μm, depending on the number of SVXII tracks associated with the primary vertex and the event topology.

Muon pairs arising from cascade decays of a single b quark are removed by selecting dimuon candidates with invariant mass greater than 5 GeV/c^2. We also reject muon

pairs with invariant mass larger than 80 GeV/c^2 that are mostly contributed by Z^0 decays.

IV. METHOD OF ANALYSIS

For muons originating from the decay of long-lived particles, the impact parameter is $d = |\beta\gamma ct \sin(\delta)|$, where t is the proper decay time of the parent particle from which the muon track originates, δ is the decay angle of the muon track with respect to the direction of the parent particle, and $\beta\gamma$ is the Lorentz boost factor. The impact parameter distribution of muon tracks is proportional to the lifetime of the parent particle. The markedly different distributions for muons from b decays, c decays, and other sources allow the determination of the parent fractions.

We determine the $b\bar{b}$ and $c\bar{c}$ content of the data following the method already used in Refs. [22,25]. The procedure is to fit the observed impact parameter distribution of the muon pairs with the expected impact parameter distributions of leptons from various sources. After data selection, the main sources of reconstructed muons are semileptonic decays of bottom and charmed hadrons, prompt decays of quarkonia, and Drell-Yan production.

Monte Carlo simulations are used to model the impact parameter distributions of muons from b- and c-hadron decays. We use the HERWIG Monte Carlo program [15], the settings of which are described in Appendix A, to generate hadrons with heavy flavors that are subsequently decayed using the EVTGEN Monte Carlo program [39]. The detector response to particles produced by the above generators is modeled with the CDF II detector simulation that in turn is based on the GEANT Monte Carlo program [40]. Impact parameter distributions of muon tracks in simulated b- and c-hadron decays are shown in Fig. 1. Since lifetimes of bottom and charmed hadrons ($c\tau_B \simeq 476$ μm and $c\tau_C \simeq 213$ μm) are much larger than the average SVXII impact parameter resolution ($\simeq 28$ μm), the dominant factor determining the impact parameter distribution is the kinematics of the semileptonic decays which is well modeled by the EVTGEN program. The impact parameter distribution of muons from prompt sources, such as quarkonia decays and Drell-Yan production, is constructed using muons from $\Upsilon(1S)$ decays (see Fig. 2). Muons from π and K in-flight decays are also regarded as prompt tracks since the track reconstruction algorithm rejects those with appreciable kinks. Tracks associated with π and K mesons which mimic the lepton signal (fake muons) are mostly prompt. The small contribution to fake muons of pion and kaon tracks arising from the decay of hadrons with heavy flavor is evaluated separately in Sec. V B. Since there are two muons in an event, the fit is performed in the two-dimensional space of impact parameters. Each axis represents the impact parameter of one of the two muons. In filling the histograms, the muon assignment is randomized. The two-dimensional impact parameter technique exploits the fact that muon impact parameters are independent uncorrelated variables.[6] The two-dimensional template distributions for each type of event are made by combining the relevant one-dimensional distributions in Fig. 1.

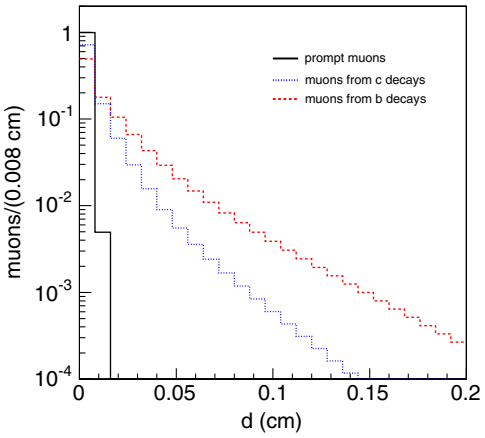

FIG. 1 (color online). Impact parameter distributions of muons coming from b- and c-hadron decays (simulation) and of prompt muons (data). Distributions are normalized to unit area.

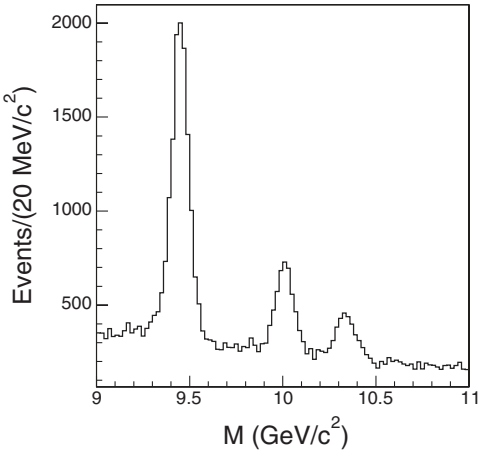

FIG. 2. Distribution of the invariant mass of muon pairs in the Υ region. The prompt template in Fig. 1 is derived using muons with invariant mass between 9.28 and 9.6 GeV/c^2. The background is sideband subtracted using dimuons with invariant mass between 9.04 and 9.2 GeV/c^2 and between 9.64 and 9.8 GeV/c^2.

We use a binned maximum log likelihood method [41] to fit the dimuon impact parameter distribution. The likelihood function L is defined as

$$L = \prod_i \prod_j [l_{ij}^{n(i,j)} e^{-l_{ij}} / n(i,j)!] \quad (1)$$

where $n(i, j)$ is the number of events in the (i, j)-th bin. The function l_{ij} is defined as

[6]The correlation between the two impact parameters, $\rho = \frac{\iint (d_1 - \langle d_1 \rangle)(d_2 - \langle d_2 \rangle) \delta d_1 \delta d_2}{\sigma_{d_1} \sigma_{d_2}}$, is approximately 0.01 in the data and the heavy flavor simulation.

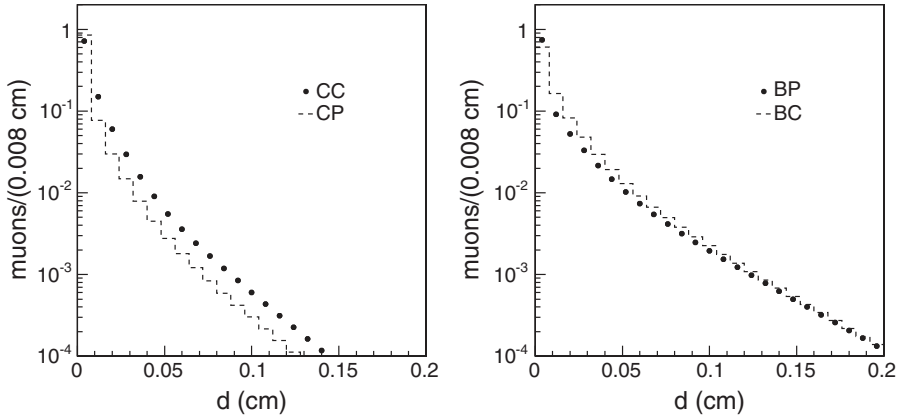

FIG. 3. Projections of the two-dimensional impact parameter distributions of some components used to fit the dimuon data (see text).

$$l_{ij} = BB \cdot S_b(i) \cdot S_b(j) + CC \cdot S_c(i) \cdot S_c(j) + PP \cdot S_p(i) \cdot S_p(j) + 0.5 \cdot [BP \cdot (S_b(i) \cdot S_p(j) + S_p(i) \cdot S_b(j)) + CP \cdot (S_c(i) \cdot S_p(j) + S_p(i) \cdot S_c(j)) + BC \cdot (S_b(i) \cdot S_c(j) + S_c(i) \cdot S_b(j))] \quad (2)$$

where S_b, S_c, and S_p are the impact parameter templates shown in Fig. 1. The fit parameters BB, CC, and PP represent the $b\bar{b}$, $c\bar{c}$, and prompt dimuon contributions, respectively. The fit parameter BP (CP) estimates the number of events in which there is only one $b(c)$ quark in the detector acceptance and the second lepton is produced by the decay or the misidentification of π or K mesons.[7] The fit parameter BC estimates the number of events in which both bottom and charmed quarks are final state partons of the hard scattering. According to the simulation, the BC component is $\simeq 4.6\%$ of the BB component and the CP component is $\simeq 83\%$ of the BP component.[8] Figure 3 shows projections of the two-dimensional distributions for each type of mixed contribution. By comparing with Fig. 1, one notes that the BB and PP components have impact parameter distributions markedly different from any other contribution, whereas the CC, CP, BP, and BC components have quite similar shapes. Using Monte Carlo pseudoexperiments we have verified that, as observed in previous studies [22,25], the likelihood function is not capable of disentangling these four components. Therefore, Eq. (1) is supplemented with the term

$$0.5 \cdot \left(\frac{(CP - 0.83 \cdot BP)^2}{(CP + 0.83^2 \cdot BP + (0.14 \cdot BP)^2)} + \frac{(BC - 0.046 \cdot BB)^2}{(BC + 0.046^2 \cdot BB + (0.013 \cdot BB)^2)} \right) \quad (3)$$

that constrains the ratios CP/BP and BC/BB to the values predicted by the simulation within their theoretical uncertainties approximated with Gaussian functions.[9]

V. HEAVY FLAVOR COMPOSITION OF THE DIMUON SAMPLE

In this section, we first determine the dimuon sample composition by fitting the impact parameter distribution with the templates described in the previous section. We then evaluate and remove the contribution of muons faked by pion or kaon tracks from heavy flavor decays. Lastly, we estimate the systematic uncertainty of the result due to the fit likelihood function and simulated templates.

A. Result of the fit to the impact parameter distribution

The two-dimensional impact parameter distribution of the 161 948 muon pairs selected in this analysis is plotted in Fig. 4(a). An appreciable fraction of events cluster along the diagonal line $d_1 = d_2$. These events are due to cosmic rays and we remove them by requiring the azimuthal angle between muons with opposite charge to be smaller than 3.135 radians (see Fig. 4(b)). In the simulation, the $\delta\phi \leq$

[7] According to the simulation, approximately 86% of the $b\bar{b}$ and $c\bar{c}$ events with an identified muon from heavy flavor decay do not contain a second hadron with heavy flavor in the detector acceptance. Therefore, following the procedure of Ref. [25], we start by ignoring the small fake muon contribution due to π and K mesons from heavy flavor decays, that is estimated in Sec. V B.

[8] In the simulation, events containing a muon from heavy flavor decay and a prompt track are mostly contributed by NLO diagrams, such as flavor excitation and gluon splitting, in which a heavy flavor quark recoils against a gluon or a light quark. The contribution of NLO terms in $c\bar{c}$ production is approximately 3.6 times larger than in $b\bar{b}$ production, but this is compensated by the kinematic acceptance for muons from c decays that is $\simeq 23\%$ of that for b decays.

[9] Using other PDF fits available in the PDF library [42], the c-to-b ratio of the flavor excitation cross section in the simulation varies up to $\pm 30\%$ [43]. The ratio of the c-to-b gluon splitting cross section also changes by $\pm 30\%$ when varying the c- and b-quark pole mass by 0.5 GeV/c^2 [43]. We use as Gaussian uncertainty the 60% variation divided by $\sqrt{12}$. The ratio of bc to $b\bar{b}$ production depends on the c-quark structure function, and varies up to $\pm 50\%$ when using other PDF fits [42].

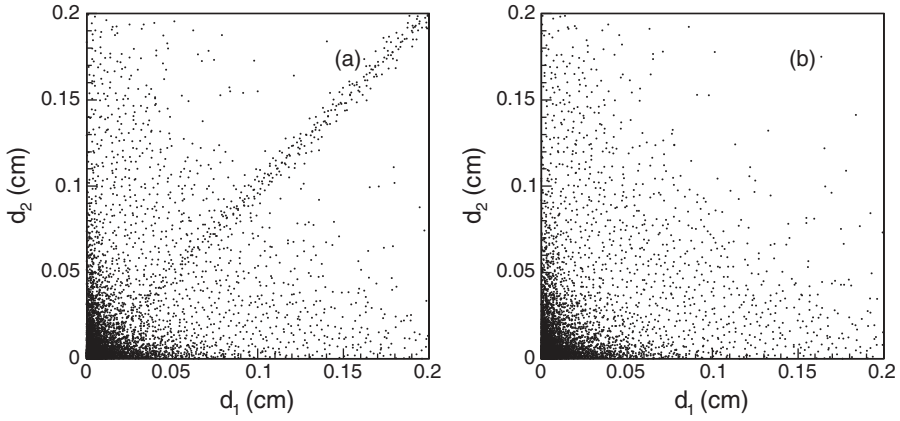

FIG. 4. Two-dimensional impact parameter distributions of muon pairs (a) before and (b) after cosmic removal.

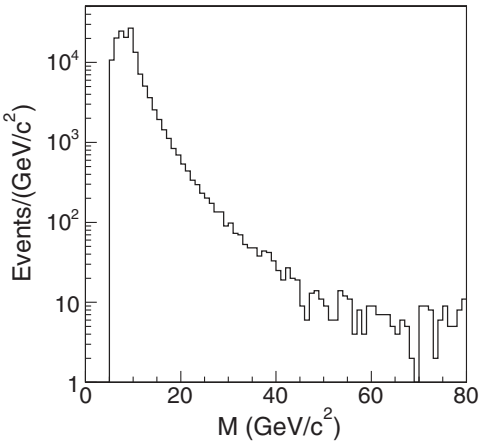

FIG. 5. Invariant mass spectrum of the muon pairs used in this study.

3.135 requirement has a 99.3% efficiency when applied to muon pairs arising from $b\bar{b}$ and $c\bar{c}$ production. The invariant mass spectrum of the remaining 143 677 events is shown in Fig. 5.

The result of the fit to the two-dimensional impact parameter distribution of the data using the likelihood function in Eqs. (1)–(3) is shown in Table I. The parameter correlation matrix is listed in Table II. The projection of the two-dimensional impact parameter distribution is compared to the fit result in Fig. 6 and the distribution of the fit residuals is plotted in Fig. 7. The best fit returns $-\ln L = 1078$. The probability of the fit to the data is determined with Monte Carlo pseudoexperiments. In each experiment, we randomly generate different components with average size as determined by the fit to the data[10] and allow for Poisson fluctuations; the impact parameter distribution for each component is randomly generated from the corresponding templates used to fit the data. We find that 16.5% of the fits to the pseudoexperiments return a $-\ln L$ value equal or larger than 1078. The values of the different components returned by the fits to each pseudoexperiment have Gaussian distributions with sigmas equal to the corresponding errors listed in Table I. The fit result is quite insensitive to the constraint $CP/BB = 0.83 \pm 0.14$ in Eq. (3). If the uncertainty is increased from 0.14 to 0.28, the size of the BB and CC components returned by the fit changes by less than half of the corresponding errors listed in Table I. However, without this constraint, the fit returns a CC component 30% smaller than the standard fit together with a ratio $CP/BP \simeq 3.5 \pm 1.9$ that would be difficult to account for. In comparison with a previous CDF measurement [25] that uses data collected in the 1992–1995 collider run (Run I), the ratio PP/BB returned by the fit has increased from $(34 \pm 1)\%$ to $(76 \pm 2)\%$. In the present study, we do not remove Υ candidates $(13\,800 \pm 290)$

TABLE I. Number of events attributed to the different dimuon sources by the fit to the impact parameter distribution. The errors correspond to a 0.5 change of $-\ln L$.

Component	Number of Events
BB	$54\,583 \pm 678$
CC	$24\,458 \pm 1565$
PP	$41\,556 \pm 651$
BP	$10\,598 \pm 744$
CP	$10\,024 \pm 1308$
BC	2165 ± 693

TABLE II. Parameter correlation coefficients returned by the fit listed in Table I.

Component	BB	CC	PP	BP	CP
CC	−0.46				
PP	0.09	0.18			
BP	0.01	−0.43	−0.14		
CP	0.27	−0.69	−0.71	0.13	
BC	−0.42	−0.19	0.15	−0.18	−0.06

[10]We have performed 1000 pseudoexperiments starting from the following component sizes: $BB_0 = 54\,600$, $CC_0 = 24\,500$, $PP_0 = 41\,500$, $BP_0 = 10\,200$, $CP_0 = 10\,000$, and $BC_0 = 2200$.

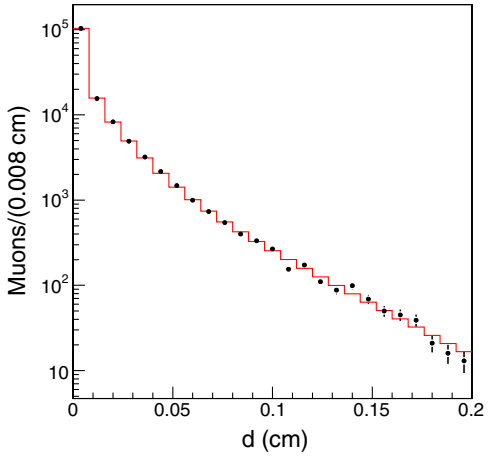

FIG. 6 (color online). The projection of the two-dimensional impact parameter distribution of muon pairs onto one of the two axes is compared to the fit result (histogram).

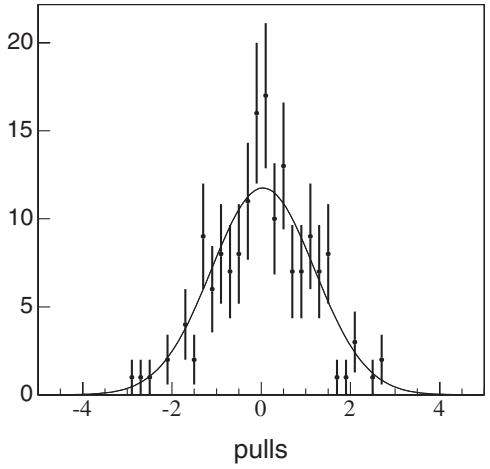

FIG. 7. Distribution of the pulls—(data-fit)/$\sqrt{\text{fit}}$—of the fit listed in Table I for the impact parameter bins with at least 10 entries. The solid line represents a fit of the pull distribution to a Gaussian function. The fit returns an average of 0.04 ± 0.10 and $\sigma = 1.06 \pm 0.09$.

which represent 32% of the PP contribution. After removing the Υ contribution, the PP contribution in the present data sample is 50% larger than in the Run I data. This is explained by a substantial increase in the rate of muons faked by prompt tracks. Therefore, in the next subsection, we evaluate the fraction of the BB yield due to muons faked by hadronic tracks from heavy flavor decays (this contribution was found negligible in the Run I data [22,25]).

B. Fake muon contribution

We use two methods to estimate the contribution of tracks arising from heavy flavor decays that mimic a CMUP signal. The first method is based on a combination of data and simulation. We use the simulation to estimate the relative yields, R_K and R_π, of $\mu - K$ and $\mu - \pi$ combinations with respect to that of real muon pairs in the decay of hadrons with heavy flavor (we select muons and tracks with $p_T \geq 3$ GeV/c and $|\eta| \leq 0.7$, and we require the invariant mass of each pair to be larger than 5 GeV/c^2). These yields are listed in Table III. The ratio of dimuons contributed by μ-track combinations to real dimuons from semileptonic decays is $F = (R_K \cdot P_f^K + R_\pi \cdot P_f^\pi)/\epsilon_\mu$, where P_f^K (P_f^π) is the probability that a pion (kaon) track mimics a muon signal. These probabilities are determined using a sample of $D^0 \rightarrow \pi K$ decays in Appendix B. The corresponding efficiency for detecting a real muon is $\epsilon_\mu = 0.5057$ (see Sec. VI). The errors in Table III are the sum in quadrature of statistical errors and the 10% systematic uncertainty of the kaon and pion rates predicted by the simulation. This systematic uncertainty is derived from a comparison of kaon and pion production rates measured at the $\Upsilon(4S)$ to the prediction of the EVTGEN Monte Carlo program [44].

We evaluate the purity $1/(1 + F)$ with a second method that is almost independent of the simulation prediction. We make use of stricter muon selection criteria by supplementing the $\Delta r\phi$ cut between the muon track projection and the CMU and CMP stubs with the requirement, referred to as χ^2 cut, that the extrapolated COT track and the CMU muon stub match within 3σ in the $r - \phi$ plane, where σ is a standard deviation that includes the effect of multiple scattering and energy loss. The efficiency of the χ^2 cut for real muons is measured using a sample of muons acquired with the J/ψ trigger. We compare the invariant mass distributions of CMUP pairs when a randomly chosen muon passes or fails the $\chi^2 \leq 9$ cut. We fit the data with two Gaussian functions to model the J/ψ signal and a straight line to model the background. The η and p_T distribution of CMUP muons from J/ψ decays are weighted to model that of muons from b-hadron decays. As shown in Fig. 8, the χ^2 cut reduces the efficiency for detecting a muon pair by $\epsilon_{\text{ineff}} = 2.20 \pm 0.04\%$.

The corresponding fake muon probabilities are measured using $D^0 \rightarrow K\pi$ decays and are discussed in Appendix B. We select a sample of dimuons enriched in fake muons by requiring $\chi^2 > 9$ for one muon and determine its heavy flavor composition by fitting the impact parameter distribution. The fit result is shown in Table IV.

TABLE III. Ratio of the numbers of $\mu - K(\pi)$ combinations to that of $\mu - \mu$ pairs, $R_{K(\pi)}$, in the simulation of different heavy flavor productions. The ratio F of the number of fake-real muon pairs to that of real dimuons is estimated using the fake muon probabilities derived in Appendix B and the measured detector efficiency $\epsilon_\mu = 0.5057$ for a real muon.

Production	R_K	R_π	F (%)
$b\bar{b}$	3.70 ± 0.43	7.58 ± 0.82	7.2 ± 0.6
$c\bar{c}$	21.73 ± 2.51	23.47 ± 2.68	32.4 ± 2.7
bc	16.78 ± 2.71	10.83 ± 2.03	21.5 ± 2.8

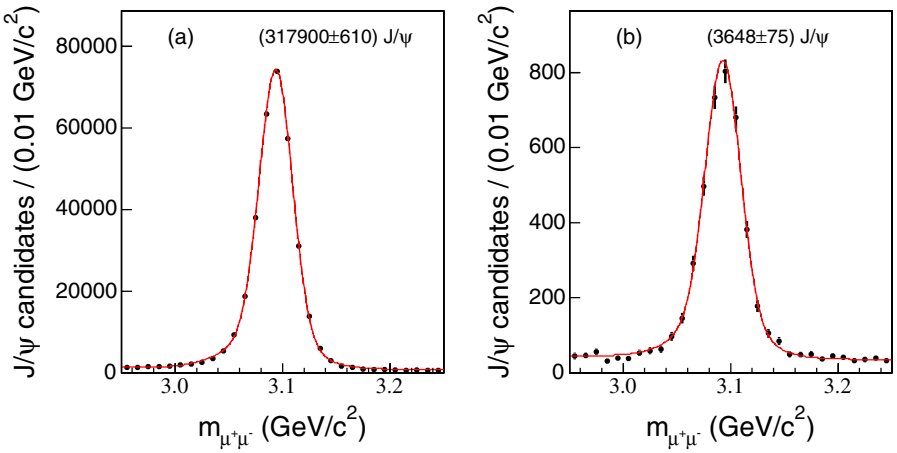

FIG. 8 (color online). Invariant mass distribution of CMUP muon pairs with a randomly chosen muon that (a) satisfies or (b) fails the $\chi^2 < 9$ requirement.

TABLE IV. Number of events attributed to the different dimuon sources by the fit to the impact parameter distribution. We use events in which at least one muon fails the $\chi^2 > 9$ requirement (see text).

Component	Number of Events
BB	1103 ± 102
CC	1189 ± 272
PP	4249 ± 131
BP	1508 ± 136
CP	1218 ± 194
BC	51 ± 15

For each heavy flavor component, we derive the fake muon contribution by solving the system of equations

$$T = HF + P_f \cdot FK, \qquad (4)$$
$$T(\chi^2 > 9) = \epsilon_{\text{ineff}} \cdot HF + P_f(\chi^2 > 9) \cdot FK,$$

where T and $T(\chi^2 > 9)$ are the size of the component determined by the fits in Table I and IV, respectively, HF is the number of real muon pairs, and FK is the number of dimuons one of which is faked by a track from heavy flavor decays. The fraction of real muon pairs reads

TABLE V. Fractions of real dimuons due to heavy flavor, $1/(1 + F)$, determined with the simulation or by using the results returned by fits to the impact parameter distributions of all muon pairs and of those pairs in which at least one muon fails the $\chi^2 \leq 9$ cut.

Production	Simulation	$\chi^2 > 9$
$b\bar{b}$	0.93 ± 0.01	1.01 ± 0.01
$c\bar{c}$	0.76 ± 0.02	0.86 ± 0.06

$$1/(1 + F) = \frac{P_f(\chi^2 > 9) \cdot T - P_f \cdot T(\chi^2 > 9)}{T \cdot (P_f(\chi^2 > 9) - 0.022 \cdot P_f)} \pm \frac{P_f}{T \cdot (P_f(\chi^2 > 9) - 0.022 \cdot P_f)} \times \sqrt{\delta T^2(\chi^2 > 9) + T^2(\chi^2 > 9)/T^2 \cdot \delta T^2}. \qquad (5)$$

This second method provides a determination of the fraction of real dimuons almost independent of the pion and kaon rate predicted by the simulation. The fraction of real muon pairs determined with the two methods is shown in Table V. We use the average and take the maximum and minimum rms deviation as systematic uncertainty (0.96 ± 0.04 for $b\bar{b}$ and 0.81 ± 0.09 for $c\bar{c}$ production). The contribution of pairs of muons that are both faked by tracks from heavy flavor decays has been estimated to be less than 0.4% in the worst case, and it is ignored.

C. Results after fake removal

Table VI lists the various heavy flavor contributions to the dimuon sample after removing the contribution of tracks from heavy flavor decays that mimic a muon signal. As shown in Table V, the contribution of muons faked by tracks from c-quark decays is not negligible. Therefore, we search the simulation for combinations of muons from b semileptonic decays and pion or kaon tracks from b- or c-quark decays (both with $p_T \geq 3$ GeV/c and $|\eta| \leq 0.7$).

TABLE VI. Number of real muon pairs from heavy flavor sources after removing the fake muon contributions. Errors include the uncertainty of the fake removal.

Component	Number of Events
BB	52 400 ± 2278
CC	19 811 ± 2540

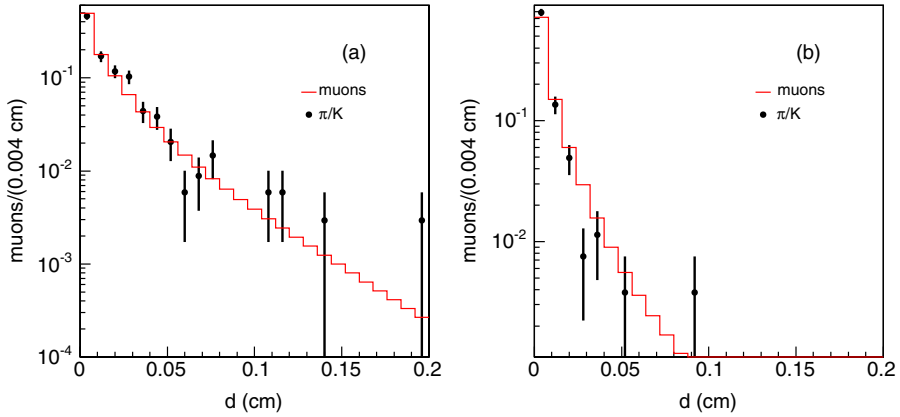

FIG. 9 (color online). Simulated impact parameter distributions of pion and kaon tracks from (a) b- and (b) c-quark decays are compared to those of muons from semileptonic decays with the same kinematical requirements.

Figure 9 compares impact parameter distributions of these tracks to the standard muon templates. Distributions for muons and hadrons are quite similar. We have fitted the data with templates that include the expected contribution of muons faked by tracks from heavy flavor decays as listed in Table V. The result of this fit differs by less than 0.1% from that of the standard fit in Table I.

For completeness, we use the simulation to verify the ratio of the BP to BB components returned by the fit performed in Sec. V. The fit yields a ratio $BP/BB = 0.194 \pm 0.013$. We search the simulation for combinations of muons from b semileptonic decays and prompt pion or kaon tracks (both with $p_T \geq 3$ GeV$/c$ and $|\eta| \leq 0.7$). The ratio of their number to that of dimuons from b semileptonic decays is 32.8 ± 0.6 (stat.). Since the efficiency for detecting a muon is $\epsilon_\mu = 0.5$ and the probability that prompt tracks fake a muon signal is 0.0032, the simulation predicts $BP/BB = 0.21 \pm 0.01$, in fair agreement with the fit result even without considering the uncertainty of the rate of prompt pions and kaons predicted by the simulation.

In $c\bar{c}$ data, approximately 20% of the muons are faked by hadronic tracks from c-quark decays. This is in agreement with the result that CP/BP is 0.95 ± 0.14 in the data and 0.83 in the heavy flavor simulation.

D. Dependence of the result on the muon p_T distribution

The impact parameter of a track arising from heavy flavor decays depends on the proper decay time of the parent hadron and the decay angle between the daughter track and the parent hadron in its rest frame. Because we select muons above a given p_T threshold, the range of accepted decay angles shrinks as the p_T difference between the daughter track and parent hadron decreases. Therefore, impact parameter templates have a small dependence on the transverse momentum distribution of muons (or parent heavy flavor) in the simulation.

In the data, we derive transverse momentum distributions for muons from b- and c-hadron decays by using the

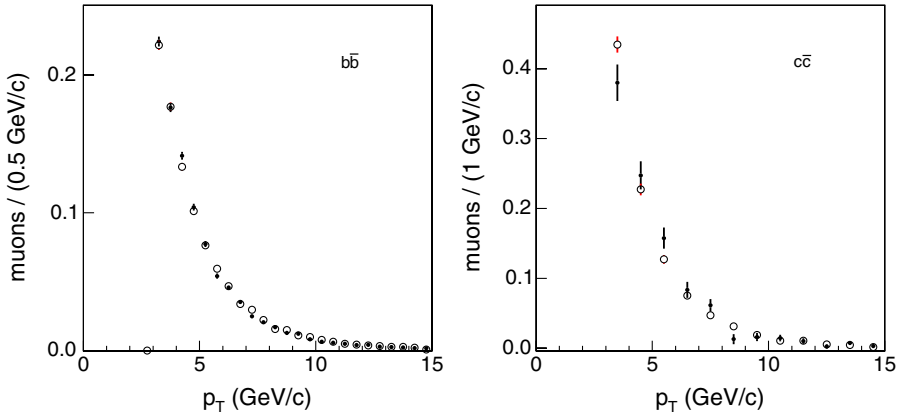

FIG. 10 (color online). Transverse momentum distributions in the data (•) and simulation (∘) for muon pairs arising from (left) $b\bar{b}$ and (right) $c\bar{c}$ production. Distributions are normalized to unit area.

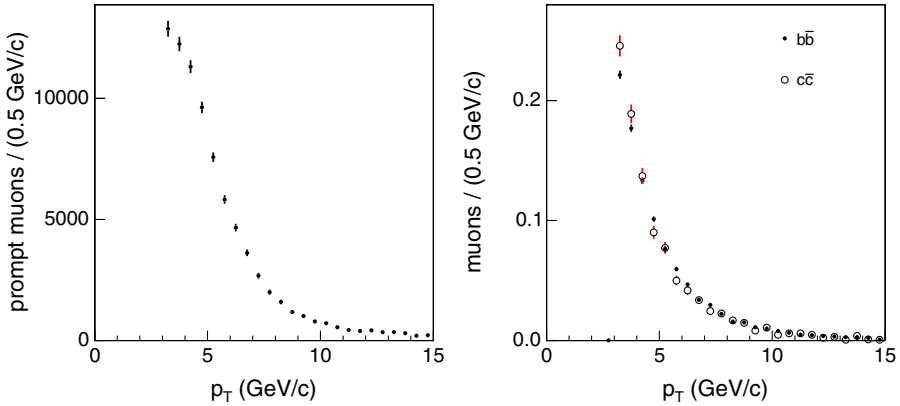

FIG. 11 (color online). Transverse momentum distribution of (left) prompt muons in the data and (right) muons from b- or c-hadron decays in the simulation. Simulated distributions are normalized to unit area.

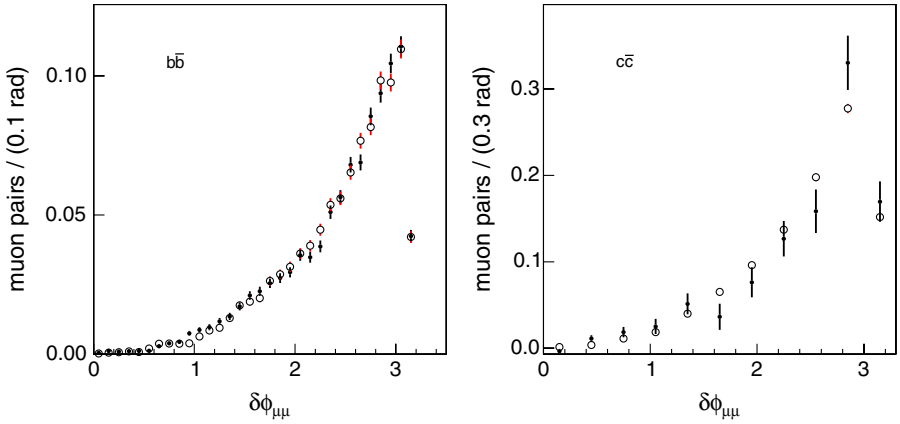

FIG. 12 (color online). Distributions of the opening azimuthal angle between two muons from (left) $b\bar{b}$ and (right) $c\bar{c}$ production in the data (•) and simulation (∘). Distributions are normalized to unit area.

${}_s\mathcal{P}lot$ statistical method [45]. We call f_n one of the six components used in the likelihood function L in Eq. (2), N_n the number of events attributed to this component by the fit in Table I, and N the total number of events.[11] Given an event e in which muons have impact parameters in the (i_e, j_e)-th bin, the probability that the event belongs to the n-th component is

$$P_n(i_e, j_e) = \frac{\sum_{l=1}^{6} V_{nl} \cdot f_l(i_e, j_e)}{\sum_{m=1}^{6} N_m \cdot f_m(i_e, j_e)}, \tag{6}$$

where

$$V_{nl}^{-1} = \frac{\sum_{e=1}^{N} f_n(i_e, j_e) \cdot f_l(i_e, j_e)}{(\sum_{m=1}^{6} N_m \cdot f_m(i_e, j_e))^2}. \tag{7}$$

The transverse momentum distribution of muons from $b\bar{b}$

[11]For example, $f_1 = S_b \cdot S_b$ and $N_1 = BB$.

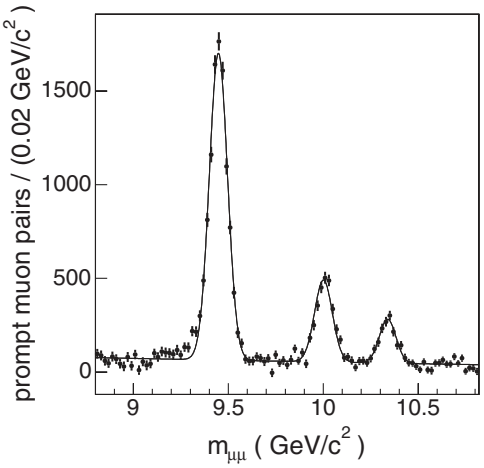

FIG. 13. Distribution of the invariant mass of the prompt dimuon component as determined by the fit to the muon impact parameter. The solid line represents a fit to the distribution that returns 9899 ± 142 $\Upsilon(1S)$ candidates, whereas the same fit to the data in Fig. 2 yields 9952 ± 122 candidates.

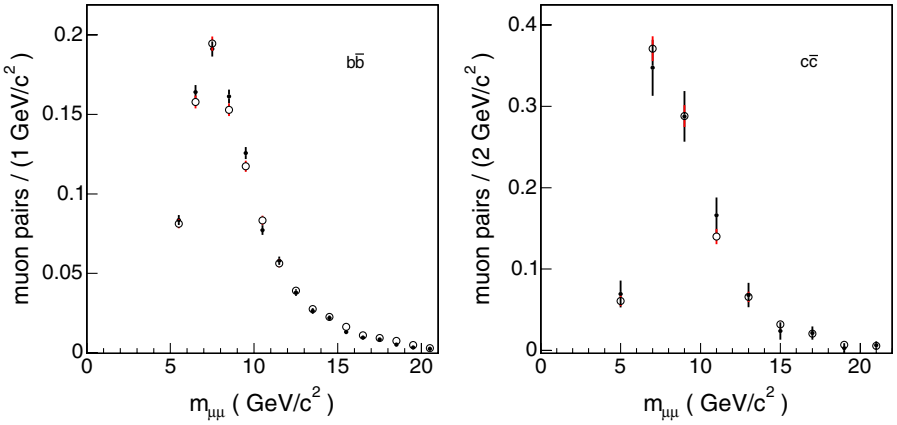

FIG. 14 (color online). Distributions of the invariant mass of muon pairs from (left) $b\bar{b}$ and (right) $c\bar{c}$ production in the data (•) and simulation (∘). Distributions are normalized to unit area.

and $c\bar{c}$ production is obtained by weighting the muon transverse momenta in the event e by the corresponding probabilities $P_1(i_e, j_e)$ and $P_2(i_e, j_e)$, respectively. The corresponding errors have been evaluated with Monte Carlo pseudoexperiments. These distributions are compared to those in the simulation in Fig. 10. The $b\bar{b}$ data are quite well modeled by the HERWIG generator. We estimate the dependence of the fit result on the muon p_T spectrum in the heavy flavor simulation by fitting the function $A \cdot p_T^{\alpha}$ to the ratio of these distributions in the simulation and in the data. The fit returns $\alpha = -0.029 \pm 0.015$. We have constructed templates by reweighting the simulated muon transverse momentum distribution with the function $p_T^{\pm 0.044}$. When these templates are used, the BB and CC yields returned by the fit change by $\pm 1.5\%$, and $\mp 4\%$, respectively. We do not correct our result for this effect, but we add this variation to other systematic effects evaluated in Sec. V E.

For completeness, we use the probability defined in Eq. (6) to show: a comparison of transverse momentum distributions of prompt muons and muons from simulated heavy flavor decays in Fig. 11; distributions of $\delta\phi$, the azimuthal opening angle between two muons, in the data and the simulation in Fig. 12; the invariant mass spectrum of the PP component in the Υ mass region in Fig. 13; and a data to simulation comparison of the invariant mass spectrum of dimuon pairs from heavy flavor decays in Fig. 14.

E. Dependence of the result on the *b*- and *c*-quark lifetime

The lifetime of the b hadron mixture with semileptonic decays produced at the Tevatron has a 0.6% uncertainty [46]. Impact parameter templates, constructed by varying the lifetime by this uncertainty, change the BB size returned by the fit by $\pm 0.4\%$ and the CC size by $\pm 1\%$. The lifetime of the c-hadron mixture has a $\pm 3.2\%$ uncertainty, mostly due to the uncertainty of the relative fractions of produced hadrons, described in Appendix A, and to the uncertainty of the semileptonic branching fractions of different c hadrons [46]. When using simulated templates constructed by changing the average lifetime by $\pm 3.2\%$, the BB size returned by the fit changes by $\pm 1\%$ and the CC size varies by $\pm 3\%$. By adding linearly these systematic uncertainties to that due to the muon p_T spectrum in the simulation, we derive a $\pm 2.9\%$ systematic error for the BB component and $\pm 8\%$ systematic error for the CC component.

VI. ACCEPTANCE AND EFFICIENCIES

The kinematic and detector acceptance is calculated with the Monte Carlo simulation described at the beginning of Sec. IV and in Appendix A. The detector response to muons produced by b- and c-hadron decays is modeled with the CDF II detector simulation that also models the L1 and L2 trigger responses. Simulated events are processed and selected with the same analysis code used for the data. The acceptance ($\mathcal{A}$) is the fraction of generated muon pairs that are identified in the detector and pass all selection requirements. At generator level, we select pairs of muons with invariant mass $5 \leq m_{\mu\mu} \leq 80$ GeV/c^2, each having $p_T \geq 3$ GeV/c and $|\eta| \leq 0.7$. Acceptances derived from the simulation are listed in Table VII. We use the data to verify the detector acceptance and efficiencies evaluated using the CDF II detector simulation. We adjust the simulation to match measurements in the data of: (1) the offline COT track reconstruction efficiency; (2) the CMUP detec-

TABLE VII. Detector and kinematic acceptances, $\mathcal{A}$, for dimuon pairs arising from $b\bar{b}$ and $c\bar{c}$ production. The acceptance $\mathcal{A}_{\text{corr}}$ includes corrections evaluated using the data.

Production	$\mathcal{A}$ (%)	$\mathcal{A}_{\text{corr}}$ (%)
$b\bar{b}$	4.21 ± 0.04	4.56 ± 0.15
$c\bar{c}$	3.95 ± 0.10	4.28 ± 0.17

TABLE VIII. Summary of efficiencies for reconstructing muon pairs from heavy flavor decays in the data and in the simulation. The last column indicates the corrections applied to the simulated efficiencies and used to derive $\mathcal{A}_{\rm corr}$ in Table VII.

Source	Data	Simulation	Correction
COT tracking	$(0.996 \pm 0.006)^2$	$(0.998 \pm 0.002)^2$	1 ± 0.013
CMUP acc. and eff.	$(0.5057 \pm 0.0032)^2$	$(0.5235 \pm 0.0022)^2$	0.933 ± 0.014
L1 CMU primitives	$(0.9282 \pm 0.0006)^2$	$(0.8489 \pm 0.0026)^2$	1.196 ± 0.007
Sili acc. and eff.	0.2365 ± 0.0013	0.2206 ± 0.0047	1.072 ± 0.024
L1 eff.	1 ± 0.001	1 ± 0.001	1 ± 0.0014
L2 eff.	$0.999\,43 \pm 0.000\,45$	0.9976 ± 0.001	1.002 ± 0.001
L3 eff.	0.90 ± 0.01	1	0.90 ± 0.01
Total	0.0471 ± 0.001	0.0435 ± 0.001	1.084 ± 0.035

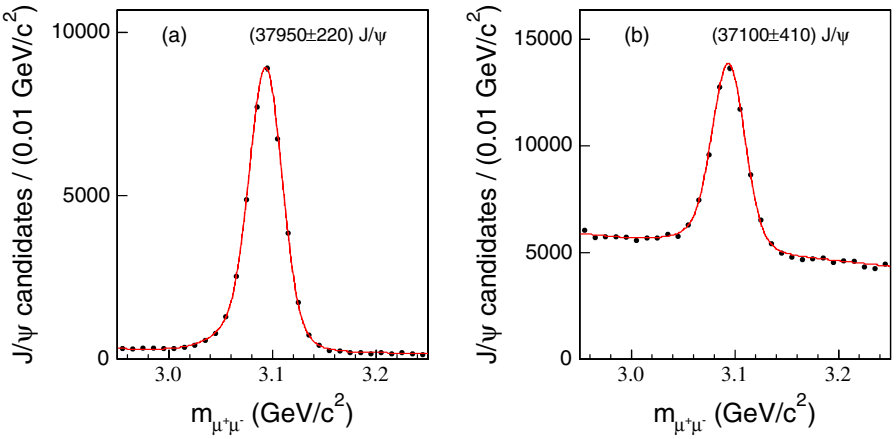

FIG. 15 (color online). Invariant mass distribution of CMUP muons paired with a displaced track (a) with or (b) without a CMUP stub. Lines represent the fits described in the text.

tor acceptance and efficiency; (3) the efficiency for finding L1 CMU primitives; (4) the SVXII acceptance and efficiency; and (5) the efficiency of the L1, L2, and L3 triggers.

In the simulation, the offline COT track reconstruction efficiency (0.998 ± 0.002) is the fraction of tracks, which at generator level satisfy the p_T and η selection cuts, that survives after selecting fully simulated events as the data. In the data, this efficiency has been measured to be 0.996 with a $\simeq 0.006$ systematic accuracy by embedding COT hits generated from simulated tracks into J/ψ data [47].[12] As in a previous study [24], we conclude that the efficiencies for reconstructing muon pairs in the data and the simulation are equal within a 1.3% systematic uncertainty.

In the simulation, the fraction of CMUP stubs generated by muon tracks with $p_T \geq 3$ GeV/c and $|\eta| \leq 0.7$ is 0.5235 ± 0.0022. In the data, this efficiency is measured by using $J/\psi \to \mu^+\mu^-$ decays acquired with the μ-SVT trigger. We evaluate the invariant mass of all pairs of a CMUP track and a track with displaced impact parameter, $p_T \geq 3$ GeV/c, and $|\eta| \leq 0.7$. We fit the invariant mass distribution with a first order polynomial plus two Gaussian functions to extract the J/ψ signal. From the number of J/ψ mesons reconstructed using displaced tracks with or without a CMUP stub (Figs. 15(a) and 15(b), respectively), we derive an efficiency of 0.5057 ± 0.0032. The integrated efficiency is evaluated after having weighted the p_T and η distributions of displaced tracks in the data to be equal to those of muons from heavy flavor decays in the simulation.

In the simulation, the efficiency for finding a L1 CMU primitive (CMU stub matched by a XFT track) is 0.8489 ± 0.0026. This efficiency is measured in the data by using events acquired with the CMUPp_T4 trigger. We combine the CMUP muon with all other CMUP muons found in the event with and without a L1 CMU primitive. We extract the number of $J/\psi \to \mu^+\mu^-$ mesons by fitting the invariant mass distributions of all candidates with a first order polynomial plus two Gaussian functions. By comparing the fitted numbers of J/ψ candidates with and without a L1

[12]The efficiency measurement was performed in a subset of the data used for this analysis. Studies of independent data samples collected in the data taking period used for this analysis show that changes of the track reconstruction efficiency are appreciably smaller than the quoted systematic uncertainty [48].

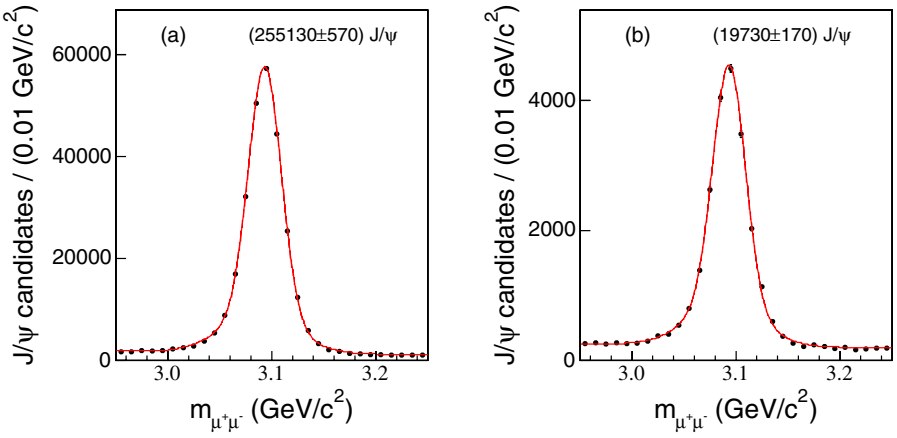

FIG. 16 (color online). Invariant mass distribution of CMUP muons paired with other CMUP muons in the event (a) with or (b) without a L1 CMU primitive. In order to derive the efficiency from the numbers of J/ψ candidates in plots (a) and (b), the histogram in (a) has an entry for each CMUP leg. Solid lines represent the fits described in the text.

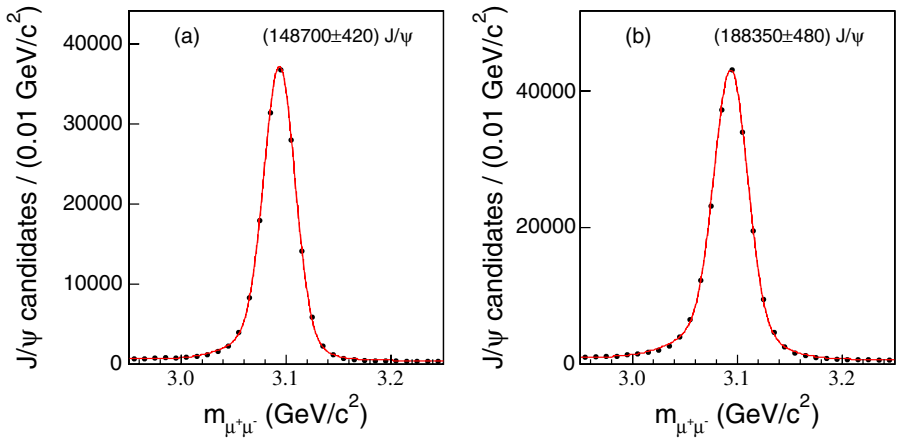

FIG. 17 (color online). Invariant mass distribution of CMUP muon pairs in which a first randomly chosen muon (a) passes or (b) fails the SVXII requirements. Solid lines represent the fits described in the text.

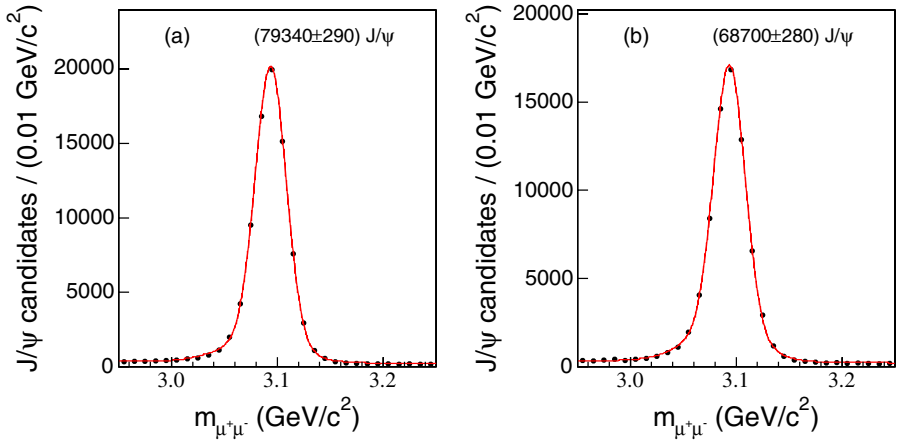

FIG. 18 (color online). Invariant mass distribution of CMUP muon pairs in which a first randomly chosen muon track satisfies the SVXII requirements and the second muon track (a) passes or (b) fails the SVXII requirements. Solid lines represent the fits described in the text.

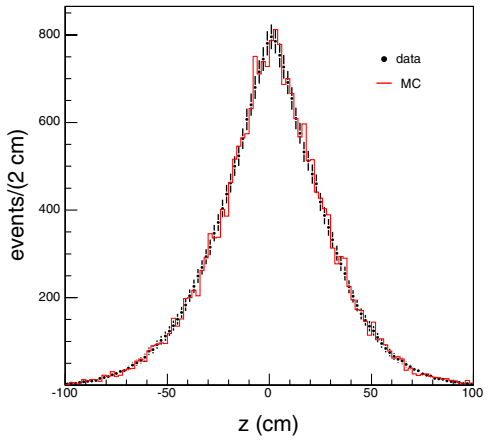

FIG. 19 (color online). Distribution of the event vertex along the beam line in the data (•) and in the heavy flavor simulation (histogram).

CMU primitive (Figs. 16(a) and 16(b), respectively) we derive an efficiency of 0.9282 ± 0.0006. The integrated efficiency is evaluated after having weighted the p_T and η distributions of the additional CMU muons to be equal to that of muons from heavy flavor decays in the simulation.

In the simulation, the probability that a CMUP pair passes the SVXII requirements described in Sec. III is 0.2206 ± 0.0047. This efficiency is measured in the data using muon pairs acquired with the J/ψ trigger. We use CMUP muons with $p_T \geq 3$ GeV/c and $|\eta| \leq 0.7$. The efficiency is evaluated in two steps. For each event, we first randomly choose a CMUP muon. After weighting the z_0 and η distributions of these muons to be equal to those of CMUP muons from simulated heavy flavor decays, we derive the SVXII efficiency ϵ_1 from the number of CMUP muons that pass or fail the SVXII requirements by fitting the dimuon invariant mass distribution with a straight line plus two Gaussian functions (see Fig. 17). For events in which the first randomly chosen muon passes the SVXII requirements, we derive the SVXII efficiency ϵ_2 from the numbers of second muons that pass or fail the SVXII requirements. After weighting the z_0 and η distributions of the second muons to be equal to those of CMUP muons from simulated heavy flavor decays, we fit again the dimuon invariant mass distributions with a straight line plus two Gaussian functions (see Fig. 18). The probability that a muon pair passes the SVXII requirements is $\epsilon_1 \cdot \epsilon_2 = 0.2365 \pm 0.0013$. This measurement of the SVXII efficiency rests on the verified assumption that the event vertex z-distribution is the same in the data and in the simulation (see Fig. 19).

In the simulation, the efficiencies of the L1 and L2 triggers are 1 and 0.9976, respectively. By using muon pairs with CMU primitives acquired with the CHARM trigger, we measure the L1 and L2 trigger efficiency to be 1 ± 0.001 and $0.999\,43 \pm 0.000\,45$, respectively. The L3 trigger is not simulated. The L3 trigger efficiency is dominated by differences between the online and offline reconstruction code efficiency.[13] The relative L3 efficiency for reconstructing a single muon identified by the offline code has been measured to be 0.997 ± 0.002 [24,47]. However, in a large fraction of the data, the L3 trigger has selected muons with the requirement that the distance between the track projection to the CMP chambers and CMP stub be $\Delta r\phi \leq 25$ cm, whereas the offline analysis requires $\Delta r\phi \leq 40$ cm. We have measured the efficiency of this L3 cut by using J/ψ candidates acquired with the J/ψ trigger that has no $\Delta r\phi$ requirement. After weighting the p_T distribution of muons from J/ψ candidates to model that of muons from b decays in the simulation, we measure the efficiency to be 0.948 ± 0.005 for a single muon. The reconstruction efficiencies in the data and in the simulation are summarized in Table VIII.

VII. DIMUON CROSS SECTION AND COMPARISON WITH PREVIOUS RESULTS

We have selected pairs of muons, each with $p_T \geq 3$ GeV/c and $|\eta| \leq 0.7$, with invariant mass $5 \leq m_{\mu\mu} \leq 80$ GeV/c^2 and produced by double semileptonic decays of heavy flavors. The production cross section is given by

$$\sigma = \frac{N}{\mathcal{L} \times \mathcal{A}_{\rm corr}}, \tag{8}$$

where $N = BB = 52\,400 \pm 2747$ for $b\bar{b}$ production ($N = CC = 19\,811 \pm 2994$ for $c\bar{c}$ production). The geometric and kinematic acceptance, $\mathcal{A}_{\rm corr}$, that includes trigger and tracking efficiencies measured with the data is listed in Table VII. The integrated luminosity of the data sample is $\mathcal{L} = 742 \pm 44$ pb^{-1}.

We derive $\sigma_{b\to\mu,\bar{b}\to\mu} = 1549 \pm 133$ pb, where the 8.6% error is the sum in quadrature of the 1.2% statistical error, the 2.9% systematic uncertainty due to the fit likelihood function, the 4.2% systematic uncertainty in the removal of the fake muon contribution, the 6% uncertainty of the luminosity, and the 3.2% uncertainty of the acceptance calculation.

We also derive $\sigma_{c\to\mu,\bar{c}\to\mu} = 624 \pm 104$ pb. In this case, the statistical error is 6.4%, the uncertainty due to the fit likelihood function is $\pm 8\%$, and the uncertainty in the removal of the fake muon contribution is 11.1%.

We evaluate the exact NLO prediction of $\sigma_{b\to\mu,\bar{b}\to\mu}$ and $\sigma_{c\to\mu,\bar{c}\to\mu}$ by complementing the MNR generator with the EVTGEN Monte Carlo program. We use the Peterson fragmentation function with $\epsilon = 0.006(0.06)$ for $b(c)$ quarks and the measured fragmentation fractions described in Appendix A. The NLO prediction is estimated using $m = 4.75(1.5)$ GeV/c^2, the factorization and normalization scale $\mu_R = \mu_F = \sqrt{p_T^2 + m^2}$, where m is the $b(c)$ quark

[13]Online algorithms are faster but less accurate than the offline reconstruction code.

mass, and the MRST PDF fits [7] (we use the five flavor scheme and $\Lambda_5 = 0.22$ GeV/c^2). In the following, we refer to it as the standard NLO calculation. We generate heavy flavor quarks with $p_T \geq 2$ GeV/c and $|y| \leq 1.3$.

The values of $\sigma_{b\to\mu,\bar{b}\to\mu}$ and $\sigma_{c\to\mu,\bar{c}\to\mu}$ predicted by the standard NLO calculation have a 2% uncertainty, estimated by using different but reasonable procedures to sum the positive and negative weights, due to real and virtual soft gluon emission, returned by the MNR computation. The theoretical prediction also carries the uncertainty of the semileptonic branching fractions $b \to \mu = 10.71 \pm 0.22$, $b \to c \to \mu = 9.63 \pm 0.44$, and $c \to \mu = 9.69 \pm 0.31\%$ [49]. In the simulation, 79.4% of the muon pairs are due to $b \to \mu$ decays, 1.3% to $b \to c \to \mu$ decays, and the rest to a mix of these decays. Therefore, the rate of predicted dimuon pairs due to $b\bar{b}$ ($c\bar{c}$) production has a 3.7% (6.4%) uncertainty. For muon pairs selected with the same kinematic cuts of the data, the standard NLO prediction is $\sigma_{b\to\mu,\bar{b}\to\mu} = 1293 \pm 55$ pb. For $c\bar{c}$ production, the standard NLO prediction is $\sigma_{c\to\mu,\bar{c}\to\mu} = 230 \pm 16$ pb.[14] The ratio of the data to the standard NLO prediction with the above mentioned uncertainties ($R1 = 1.20 \pm 0.11$ for $b\bar{b}$ production and $R1 = 2.71 \pm 0.49$ for $c\bar{c}$ production) can be used to extract the value of $\sigma_{b\bar{b}}$ and $\sigma_{c\bar{c}}$ in the data. In addition, as discussed in Sec. I, the theoretical prediction has a 15% uncertainty due to the choice of the heavy quark pole-mass,[15] PDF fits, and renormalization and factorization scales. After including the latter uncertainty, the ratio of the data to the standard NLO prediction is 1.20 ± 0.21 for $b\bar{b}$ production and 2.71 ± 0.64 for $c\bar{c}$ production.

The $c\bar{c}$ correlation measurement has no previous result to compare with. However, the CDF study in Ref. [25] has measured the ratio of dimuon pairs due to $c\bar{c}$ to those due to $b\bar{b}$ production. That study uses muon pairs selected in the same kinematic region as our measurement, and finds a ratio $CC/BB = 0.15 \pm 0.02$,[16] whereas our fit to the impact parameter distributions yields $CC/BB = 0.38 \pm 0.07$. In the simulation, this ratio is 0.17 (0.16) when using the HERWIG (MNR) generator.

The extraction of $\sigma_{b\bar{b}}$ from the dimuon production cross section and the comparison to other measurements is not a trivial issue. Muons with $p_T \geq 3$ GeV/c and $|\eta| \leq 0.7$ are mostly contributed by b quarks with $p_T \geq 6.5$ GeV/c and $|y| \leq 1$. However, there are tails contributed from b quarks with p_T as small as 2 GeV/c and $|y|$ as large as 1.3. If these contributions are included, the resulting value of $\sigma_{b\bar{b}}$ is dominated by the production of b quarks with the smallest p_T that, unfortunately, has a large statistical error because of the small kinematic acceptance. The measurement of $\sigma_{b\bar{b}}$ in Ref. [22] is based upon muon pairs selected with the same kinematic cuts as this study. That study does not report the value of $\sigma_{b\to\mu,\bar{b}\to\mu}$ but, in the assumption that these muon pairs are produced by b quarks with $p_T \geq 6.5$ GeV/c and $|y| \leq 1$, quotes $\sigma_{b\bar{b}}(p_T \geq 6.5\ \text{GeV}/c, |y| \leq 1) = 2.42 \pm 0.45\ \mu$b. It seems more appropriate to derive this cross section assuming that the ratio of data to theory is the same as that of the measured to predicted dimuon cross section. Using this method, the ratio $R1$ yields $\sigma_{b\bar{b}}(p_T \geq 6.5\ \text{GeV}/c, |y| \leq 1) = 1324 \pm 121$ nb (the standard NLO prediction is 1103 ± 169 nb). In the simulation, only 75% of the muon pairs arise from b and $\bar{b}$ quarks with $p_T \geq 6.5$ GeV/c and $|y| \leq 1$. The result of Ref. [22], rescaled by 75%, becomes $\sigma_{b\bar{b}}(p_T \geq 6.5\ \text{GeV}/c, |y| \leq 1) = 1.80 \pm 0.34\ \mu$b.

The D0 collaboration [23] has measured $\sigma_{b\to\mu,\bar{b}\to\mu} = 1027 \pm 260$ pb using muon pairs with $6 \leq m_{\mu\mu} \leq 35$ GeV/c^2. That study selects muons with $4 \leq p_T \leq 25$ GeV/c, $|\eta| \leq 0.8$, and contained in a jet with transverse energy $E_T \geq 12$ GeV. Reference [23] compares data to the exact NLO prediction that, evaluated with the HVQJET Monte Carlo program [50], is 357 pb. For this kinematical selection, except the request that muons are embedded in jets, the standard NLO prediction is $\sigma_{b\to\mu,\bar{b}\to\mu} = 550$ pb. When applying these kinematical cuts to our data, and before asking that muons are contained in jets with $E_T \geq 12$ GeV, we measure $\sigma_{b\to\mu,\bar{b}\to\mu} = 658 \pm 55$ pb.

Using the ratio $R1$, the data yield $\sigma_{b\bar{b}}(p_T \geq 6\ \text{GeV}/c, |y| \leq 1) = 1618 \pm 148$ nb. The standard NLO prediction is $\sigma_{b\bar{b}}(p_T \geq 6\ \text{GeV}/c, |y| \leq 1) = 1348 \pm 209$ nb.[17] For comparison, the HERWIG parton-level prediction is $\sigma_{b\bar{b}}(p_T \geq 6\ \text{GeV}/c, |y| \leq 1) = 1327$ nb, and the cross section returned by the MC@NLO generator[18] is $\sigma_{b\bar{b}}(p_T \geq 6\ \text{GeV}/c, |y| \leq 1) = 1704$ nb, 27% larger than the MNR result.[19]

The value of $\sigma_{b\bar{b}}$ has been extracted from the data using a fragmentation model based on the Peterson function. As previously noted, the MNR and HERWIG generators

[14]For comparison, the prediction of the HERWIG generator is $\sigma_{b\to\mu,\bar{b}\to\mu} = 904 \pm 33$ pb and $\sigma_{c\to\mu,\bar{c}\to\mu} = 173 \pm 11$ pb.

[15]Following tradition, we vary the pole mass of b quarks by ± 0.25 GeV/c^2 and that of c quarks by ± 0.2 GeV/c^2.

[16]The error is statistical. Systematic effects due to the fit likelihood functions or c-hadron lifetime were not investigated.

[17]For charmed quarks, the standard NLO prediction is $\sigma_{c\bar{c}}(p_T \geq 6\ \text{GeV}/c, |y| \leq 1) = 2133 \pm 323$ nb.

[18]We input the same b-quark mass, scales and PDF fits used in the standard NLO calculation.

[19]The total $b\bar{b}$ cross section predicted by both MC@NLO and MNR generators is 56.6 μb and compares well with the result of the NDE calculation (57.6 μb). However, the inclusive single b cross section for $p_T \geq 6$ GeV/c and $|y| \leq 1$ predicted by the NDE and MNR programs are 5.5 and 5.6 μb, respectively, whereas MC@NLO generator predicts 11.8 μb. In contrast, for both b and $\bar{b}$ quarks with $p_T \geq 25$ GeV/c and $|y| \leq 1.2$ the MC@NLO prediction is approximately 12% smaller than that of the MNR generator.

predict the same parton-level cross section $\sigma_{b\bar{b}}(p_T \geq 6\ \mathrm{GeV}/c, |y| \leq 1)$. The HERWIG generator models the b-quark fragmentation differently, and this difference results in a prediction of $\sigma_{b\to\mu,\bar{b}\to\mu}$ which is 30% smaller than that of the MNR generator implemented with the Peterson fragmentation model. In the transverse momentum range of this study, the FONLL prediction for the single b-quark cross section is fairly well reproduced by the NDE calculation when using the Peterson fragmentation function with $\epsilon = 0.002$ [11,51]. When using this fragmentation function, the exact NLO prediction becomes $\sigma_{b\to\mu,\bar{b}\to\mu} = 1543$ pb, which is 20% higher than the standard exact NLO prediction.

As argued in Ref. [52], the charmed quark production in e^+e^- data can be described at NLO accuracy using the Peterson fragmentation model with $\epsilon = 0.02$. In this case, the NLO prediction becomes $\sigma_{c\to\mu,\bar{c}\to\mu} = 383$ pb, 66% larger than the standard NLO prediction. When using the smaller values of the ϵ parameter, the ratio of data to theory becomes 1.0 ± 0.2 for $\sigma_{b\to\mu,\bar{b}\to\mu}$ and 1.6 ± 0.4 for $\sigma_{c\to\mu,\bar{c}\to\mu}$.

VIII. CONCLUSIONS

We have measured the production cross section of muon pairs from double semileptonic decays of b and $\bar{b}$ quarks produced at the Tevatron Fermilab collider operating at $\sqrt{s} = 1.96$ TeV. We select muons with $p_T \geq 3\ \mathrm{GeV}/c$ and $|\eta| \leq 0.7$. We select dimuons with $5 \leq m_{\mu\mu} \leq 80\ \mathrm{GeV}/c^2$ to reject the contribution of sequential decays of single b quarks and Z^0 decays. The main sources of these muon pairs are semileptonic decays of b and c quarks, prompt decays of quarkonia, and Drell-Yan production. We determine the $b\bar{b}$ content of the data by fitting the impact parameter distribution of muon tracks with the templates expected for the various sources. Previous measurements of the $b\bar{b}$ correlations at the Tevatron yield contradictory results. The ratio of the data to exact NLO prediction is approximately 1.15 ± 0.21 when b quarks are selected via secondary vertex identifications, whereas this ratio is found to be significantly larger than 2 when identifying b quarks through their semileptonic decays.

We measure $\sigma_{b\to\mu,\bar{b}\to\mu} = 1549 \pm 133$ pb. The exact NLO prediction is evaluated using the MNR calculation complemented with the EVTGEN generator. In the calculation, we use $m_b = 4.75\ \mathrm{GeV}/c^2$, the factorization and normalization scale $\mu_R = \mu_F = \sqrt{p_T^2 + m_b^2}$, and the MRST PDF fits (we use the five flavor scheme and $\Lambda_5 = 0.22\ \mathrm{GeV}/c^2$). We use the Peterson fragmentation function with $\epsilon = 0.006$, and the PDG values for the fragmentation fractions. The NLO prediction is $\sigma_{b\to\mu,\bar{b}\to\mu} = 1293 \pm 201$ pb. The ratio of the data to the NLO prediction is 1.20 ± 0.21.

From this measurement, we also derive $\sigma_{b\bar{b}}(p_T \geq 6\ \mathrm{GeV}/c, |y| \leq 1) = 1618 \pm 148$ nb (the exact NLO prediction is 1348 ± 209 nb). The extraction of $\sigma_{b\bar{b}}$ from the data depends on the choice of the fragmentation functions that connect a muon to the parent b quark. No fragmentation functions are available that match the accuracy of the NLO calculation. Reasonable changes of the fragmentation model indicate that the value of $\sigma_{b\bar{b}}$ extracted from the data has an additional uncertainty of approximately 25%.

ACKNOWLEDGMENTS

We thank the Fermilab staff and the technical staffs of the participating institutions for their vital contributions. This work was supported by the U.S. Department of Energy and National Science Foundation; the Italian Istituto Nazionale di Fisica Nucleare; the Ministry of Education, Culture, Sports, Science and Technology of Japan; the Natural Sciences and Engineering Research Council of Canada; the National Science Council of the Republic of China; the Swiss National Science Foundation; the A. P. Sloan Foundation; the Bundesministerium für Bildung und Forschung, Germany; the Korean Science and Engineering Foundation and the Korean Research Foundation; the Particle Physics and Astronomy Research Council and the Royal Society, UK; the Institut National de Physique Nucleaire et Physique des Particules/CNRS; the Russian Foundation for Basic Research; the Comisión Interministerial de Ciencia y Tecnología, Spain; the European Community's Human Potential Programme; the Slovak R&D Agency; and the Academy of Finland.

APPENDIX A: SETTINGS OF THE HERWIG MONTE CARLO PROGRAM

We generate generic $2 \to 2$ hard scattering, process 1500, using version 6.5 of the HERWIG Monte Carlo program. In the generic hard parton scattering, $b\bar{b}$ and $c\bar{c}$ pairs are generated by HERWIG through processes of order α_s^2 (LO) such as $gg \to b\bar{b}$ (direct production). Processes of order α_s^3 are implemented in HERWIG through flavor excitation processes, such as $gb \to gb$, or gluon splitting, in which the process $gg \to gg$ is followed by $g \to b\bar{b}$. We generate final state partons with $p_T \geq 5\ \mathrm{GeV}/c^2$ and $|y| \leq 1.7$. The hard scattering cross section is evaluated using the MRST fits to the parton distribution functions [7]. Hadrons with heavy flavor, produced by the HERWIG generator, are decayed with the EVTGEN Monte Carlo tuned by the *BABAR* collaboration [39]. We retain simulated events that contains a pair of muons, each of them with $p_T \geq 2.8\ \mathrm{GeV}/c^2$ and $|\eta| \leq 0.8$.[20] We find one good event in approximately 10^8 generated events. These events are used to determine the kinematical and detector acceptance as well as the impact parameter templates used to extract the

[20]We also produced simulated samples requiring the presence of only one muon or no muons at all.

heavy flavor composition of the data. Since different b hadrons, and especially different c hadrons, have quite different lifetimes and semileptonic branching fractions, it is important that the generator models correctly the known fragmentation fractions and functions of b and c quarks. The HERWIG generator makes use of a large number of parameters that can be adjusted to this purpose. Unfortunately, their default setting [53] does not yield a satisfactory modeling of the heavy quark fragmentation that we have studied by comparing simulated Z^0 decays (process 2160 of HERWIG) to e^+e^- data. The available parameters do not allow us to tune the ratio of baryon to mesons simultaneously for bottom and charmed flavors, nor to reproduce the measured ratio of vector to pseudoscalar resonances produced in the heavy quark hadronization. The first deficiency becomes a problem when the simulation of a QCD process, such as ours, is extremely time consuming. The second deficiency impacts the evaluation of the kinematical efficiency and lifetime templates for c quarks because D^* mesons mostly decay to D^0 mesons, the lifetime and semileptonic branching fractions of which differ by a factor of 3 from that of D^+ mesons. We have solved these issues by adding two additional parameters, analogous of CLPOW. In the HWUINC.F routine of the HERWIG program, the parameter CLPOW tunes the invariant mass distribution of cluster generated in the heavy quark hadronization. We use this parameter for b quarks only. For c quarks, the parameter CLPOW is replaced with two parameters, LCLPW and DCLPW, that separately control the yield of c-quark (mesons) and c-diquark (baryons) clusters, respectively. Table IX lists the HERWIG parameter settings used in our simulation. Table X compares fragmentation fractions in the tuned simulation at the

TABLE IX. Parameter settings used in our simulation are compared to the HERWIG default values.

Parameter	Default	This Study
QCDLAM	0.180	0.18
RMASS (4) (c quark)		1.50
RMASS (5) (b quark)		4.75
RMASS (13)	0.75	0.75
CLMAX	3.35	3.75
CLPOW	2.00	1.06
LCLPW		2.20
DCLPW		1.30
PSPLT (1)	1.00	0.50
PSPLT (2)	1.00	1.10
CLSMR (1)	0.00	0.00
CLSMR (2)	0.00	0.40
PWT (3)	1.00	0.70
PWT (7)	1.00	0.45
SNGWT	1.00	1.00
DECWT	1.00	1.00
REPWT (0, 1, 0)	1.00	10.00

TABLE X. Fragmentation fractions in the tuned HERWIG simulation are compared to data. The fragmentation fractions of b quarks (first three rows) are defined according to the PDG notation [46].

		Data	HERWIG
$f_u = f_d$	=	$(39.7 \pm 1.0)\%$	39.6%
f_s	=	$(10.7 \pm 1.1)\%$	11.2%
f_{baryon}	=	$(9.9 \pm 1.7)\%$	9.6%
$f(c \to D^+) = f(c \to D^0)$	=	$(16.4 \pm 2.3)\%$	16.9%
$f(c \to D^{*+}) = f(c \to D^{*0})$	=	$(22.8 \pm 2.5)\%$	22.5%
$f(c \to D_s + D_s^*)$	=	$(12.1 \pm 2.5)\%$	11.5%
$f(c \to \text{baryons})$	=	$(9.5 \pm 4.0)\%$	9.7%

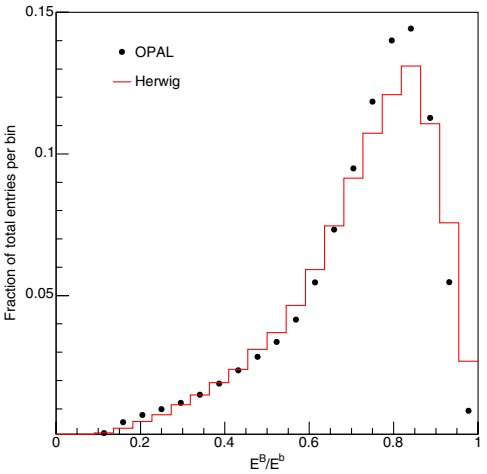

FIG. 20 (color online). Distribution of ratio of the energy carried by all B hadrons to that of the parent b quarks. The data are OPAL measurements at the Z pole [59], while the HERWIG distribution is obtained with the parameter tuning listed in Table IX.

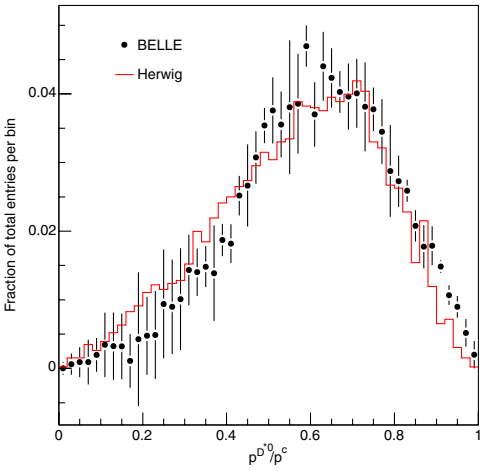

FIG. 21 (color online). Distribution of ratio of the momentum carried by D^* mesons to that of the parent c quarks. The data are BELLE measurements [54], while the HERWIG distribution is obtained with the parameter tuning listed in Table IX.

Z-pole to the data. The fragmentation fractions for b quarks are taken from Ref. [46]. For c quarks, the fragmentation fractions are taken from Refs. [54–58]. The fragmentation functions are tuned in the HERWIG simulation by adjusting the parameters PSPLT and CLSMR to the values listed in Table IX. Figures 20 and 21 compare some fragmentation functions predicted by the tuned HERWIG simulation to data. Simulated fragmentation functions are derived using Z^0 decays generated with process 2160. Figure 20 compares the distribution of the fraction of energy of parent b quarks carried by all B hadrons resulting from the heavy quark fragmentation to OPAL data [59] that in turn are consistent with Aleph and SLD measurements [60,61]. Figure 21 compares the fraction of momentum of the parent c quarks carried by D^* mesons to BELLE data [54] that in turn are consistent with the CLEO result [55] and the Aleph measurement at the Z-pole [62]. The data are fairly well modeled by the HERWIG generator with the parameter settings listed in Table IX. A similar agreement for the fragmentation functions, but not the fragmentation fractions, can be achieved using the tuning proposed by some of the HERWIG authors [63].

APPENDIX B: RATE OF FAKE MUONS

Muons reconstructed in the CMUP detector are divided in this study into real and fake muons. Real muons originate from semileptonic decays of hadrons with heavy flavor, the Drell-Yan process, and Υ decays. Fake muons include muons from π or K decays and hadronic punchthroughs that mimic a muon signal. The probability that a π or K track is misidentified as a muon is evaluated using $D^0 \rightarrow K\pi$ decays reconstructed in data collected with the CHARM trigger. We select oppositely charged particles, each with $p_T \geq 3$ GeV/c and $|\eta| \leq 0.7$, with $|\delta z_0| \leq 0.5$ cm. We require that each track is reconstructed in the

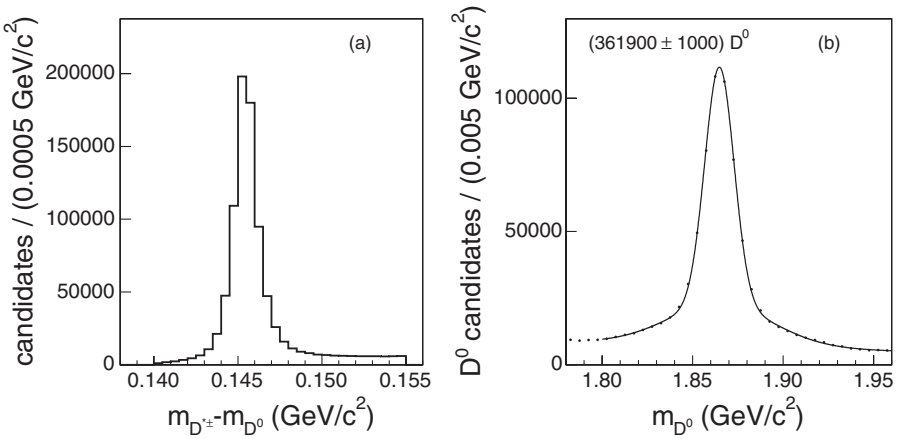

FIG. 22. Distributions of (a) $m_{D^{*\pm}} - m_{D^0}$ and (b) the invariant mass of D^0 candidates (the solid line represents the fit described in the text).

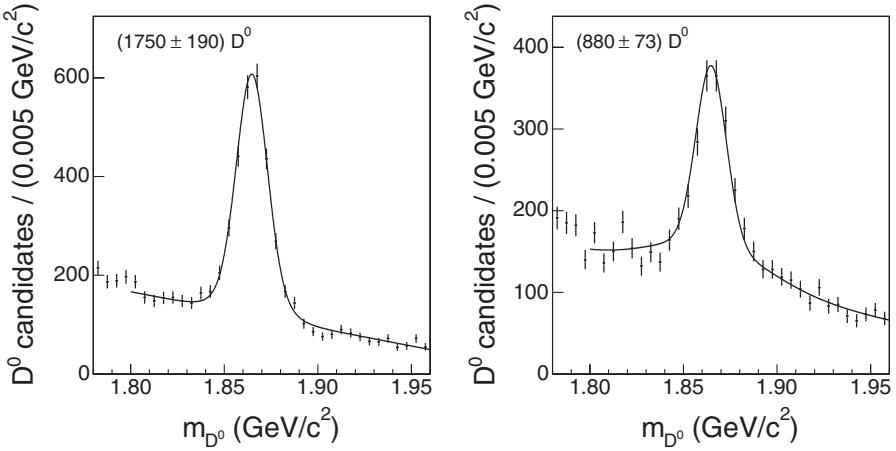

FIG. 23. Invariant mass distribution of D^0 candidates with (left) a kaon or (right) a pion leg identified as a CMUP muon. Solid lines represent the fits described in the text.

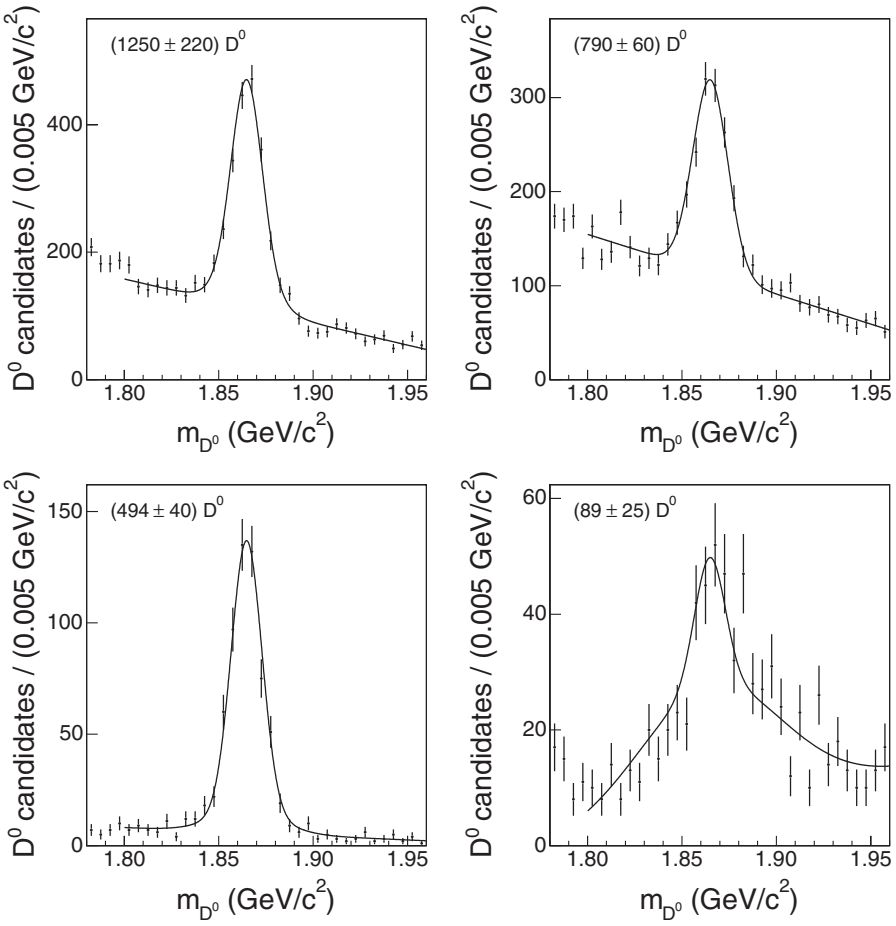

FIG. 24. Invariant mass distribution of D^0 candidates with (left) a kaon or (right) a pion leg identified as a CMUP muon. Top (bottom) plots require muons passing (failing) the $\chi^2 < 9$ cut. Solid lines represent the fits described in the text.

microvertex detector with hits in at least four of the eight silicon layers. We evaluate the pair invariant mass for all pion-kaon mass assignments. The invariant mass is evaluated by constraining the two tracks to originate from a common point in the three-dimensional space (vertex constraint). We reject pairs if the probability of originating from a common vertex is smaller than 0.0002 or their invariant mass is outside the interval 1.77–1.97 GeV$/c^2$. We also require that the displacement of the D^0-candidate vertex from the primary event vertex, projected onto the D^0 transverse momentum vector, be larger than 0.02 cm. To further reduce the combinatorial background, we also require the D^0 candidate to originate from a $D^{*\pm}$ decay. We reconstruct $D^{*\pm}$ decays by combining D^0 candidates with all additional COT tracks with a distance $|\delta z_0| \leq 0.5$ cm with respect to the D^0 vertex. Additional tracks are assumed to be pions and the D^* invariant mass is evaluated by vertex constraining pion and D^0 candidates and rejecting combinations with probability smaller than 0.0002. The observed $m_{D^{*\pm}} - m_{D^0}$ distribution is shown in Fig. 22(a). We retain D^0 candidates with $0.144 \leq m_{D^{*\pm}} - m_{D^0} \leq 0.147$ (their invariant mass distribution is plotted in Fig. 22(b)). The fake muon probability is derived using the invariant mass spectrum of $D^0 \rightarrow \pi K$ decays in which one of the decay products is matched to a CMUP stub (see Fig. 23). We fit the data with two Gaussian functions to model the D^0 signal and a polynomial function to model the underlying background. The Gaussian functions model separately the right and wrong sign D^0 decays. In the fits to the data in Fig. 23, the width and peak of the first Gaussian function and the peak of the second one are constrained to the value returned by the best fit to the data in Fig. 22(b) (peak at 1.865 GeV$/c^2$ and $\sigma = 0.008$ GeV$/c^2$). Using the same method, we also evaluate the rate of fake

TABLE XI. Probabilities, P_f^K and P_f^π, that pions and kaons, respectively, mimic a CMUP signal for different selection criteria.

CMUP selection	P_f^K (%)	P_f^π (%)
Standard	0.483 ± 0.003	0.243 ± 0.004
$\chi^2 \leq 9$	0.347 ± 0.003	0.219 ± 0.003
$\chi^2 > 9$	0.136 ± 0.001	0.025 ± 0.002

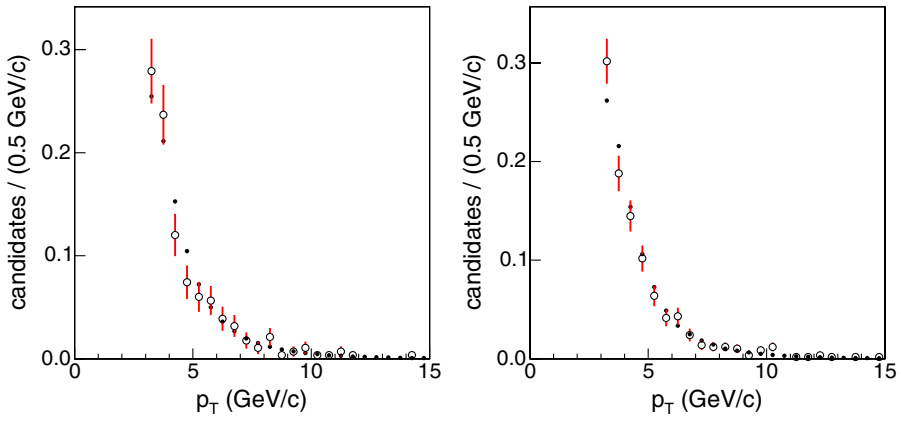

FIG. 25 (color online). Transverse momentum distributions of (left) kaons and (right) pions from D^0 decays (∘) are compared to those of tracks (•) arising from simulated b-hadron decays.

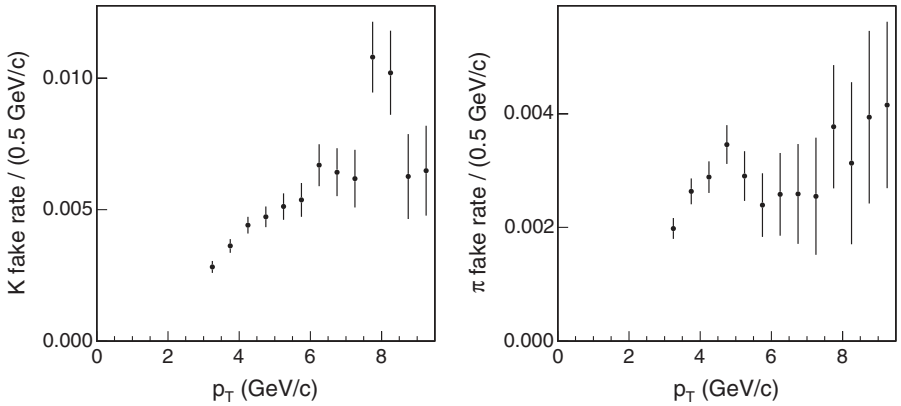

FIG. 26. Fake muon probability as a function of the (left) kaon and (right) pion transverse momentum.

CMUP muons that pass or fail the stricter $\chi^2 \leq 9$ selection cut described in Sec. V B (see Fig. 24). By using 361 902 $D^0 \rightarrow K\pi$ candidates we measure the fake muon probabilities listed in Table XI. The fake muon probabilities have been evaluated after weighting the transverse momentum distributions of kaons (pions) from D^0 decays to model that of kaons (pions) produced by simulated b-hadron decays (unweighted distributions are shown in Fig. 25). Since the fake muon probability is not a strong function of the transverse momentum (see Fig. 26), we ignore the statistical uncertainty of the simulated distributions because its effect is negligible compared to the 10% uncertainty of the kaon and pion rates predicted by the simulation.

[1] M. L. Mangano, P. Nason, and G. Ridolfi, Nucl. Phys. **B373**, 295 (1992). The FORTRAN code, also referred to as HVQMNR, is made available by the authors and can be downloaded from http://www.ge.infn.it/~ridolfi.
[2] P. Nason, S. Dawson, and R. K. Ellis, Nucl. Phys. **B327**, 49 (1989); **B335**, 260 (1990).
[3] S. Frixione *et al.*, Adv. Ser. Dir. High Energy Phys. **15**, 609 (1998).
[4] M. Cacciari *et al.*, J. High Energy Phys. 07 (2004) 033.
[5] D. Acosta *et al.*, Phys. Rev. D **69**, 072004 (2004).
[6] F. Happacher *et al.*, Phys. Rev. D **73**, 014026 (2006); Proceedings of DIS 2006, Tsukuba, Japan, http://www-conf.kek.jp/dis06/doc/WG5/hfl20-happacher.ps (unpublished).
[7] A. D. Martin *et al.*, Eur. Phys. J. C **4**, 463 (1998).
[8] J. Pumplin *et al.*, J. High Energy Phys. 07 (2002) 012.
[9] C. Peterson *et al.*, Phys. Rev. D **27**, 105 (1983).
[10] J. Chrin, Z. Phys. C **36**, 163 (1987).
[11] M. Cacciari and P. Nason, Phys. Rev. Lett. **89**, 122003 (2002).
[12] M. Cacciari *et al.*, J. High Energy Phys. 05 (1998) 007.

[13] P. Nason and C. Oleari, Nucl. Phys. **B565**, 245 (2000); B. Mele and P. Nason, Nucl. Phys. **B361**, 626 (1991); G. Colangelo and P. Nason, Phys. Lett. B **285**, 167 (1992).
[14] H. Heister *et al.*, Phys. Lett. B **512**, 30 (2001); K. Abe *et al.*, Phys. Rev. D **65**, 092006 (2002).
[15] G. Marchesini and B. R. Webber, Nucl. Phys. **B310**, 461 (1988); G. Marchesini *et al.*, Comput. Phys. Commun. **67**, 465 (1992).
[16] T. Sjöstrand and M. Bengtsson, Comput. Phys. Commun. **43**, 367 (1987); H. Bengtsson and T. Sjöstrand, Comput. Phys. Commun. **46**, 43 (1987).
[17] S. Frixione *et al.*, J. High Energy Phys. 08 (2003) 007; S. Frixione and B. R. Webber, J. High Energy Phys. 06 (2002) 029. The code is made available by the authors and can be downloaded from http://www.hep.phy.cam.ac.uk/theory/webber/MCatNLO/.
[18] P. Nason *et al.*, arXiv:hep-ph/0003142.
[19] S. Alekhin *et al.*, arXiv:hep-ph/0204316.
[20] T. Shears, Proc. Sci., HEP2005 (2005) 072.
[21] F. Abe *et al.*, Phys. Rev. D **53**, 1051 (1996).
[22] F. Abe *et al.*, Phys. Rev. D **55**, 2546 (1997).
[23] B. Abbott *et al.*, Phys. Lett. B **487**, 264 (2000).
[24] A. Abulencia *et al.*, Phys. Rev. D **75**, 012010 (2007).
[25] D. Acosta *et al.*, Phys. Rev. D **69**, 012002 (2004).
[26] F. Abe *et al.*, Nucl. Instrum. Methods Phys. Res., Sect. A **271**, 387 (1988).
[27] R. Blair *et al.*, Fermilab Report No. FERMILAB-Pub-96/390-E, 1996.
[28] C. S. Hill *et al.*, Nucl. Instrum. Methods Phys. Res., Sect. A **530**, 1 (2004).
[29] A. Sill *et al.*, Nucl. Instrum. Methods Phys. Res., Sect. A **447**, 1 (2000).
[30] T. Affolder *et al.*, Nucl. Instrum. Methods Phys. Res., Sect. A **453**, 84 (2000).
[31] T. Affolder *et al.*, Nucl. Instrum. Methods Phys. Res., Sect. A **526**, 249 (2004).
[32] G. Ascoli *et al.*, Nucl. Instrum. Methods Phys. Res., Sect. A **268**, 33 (1988).
[33] J. Elias *et al.*, Nucl. Instrum. Methods Phys. Res., Sect. A **441**, 366 (2000).
[34] D. Acosta *et al.*, Nucl. Instrum. Methods Phys. Res., Sect. A **461**, 540 (2001).
[35] R. Downing *et al.*, Nucl. Instrum. Methods Phys. Res., Sect. A **570**, 36 (2007).
[36] M. M. Block and R. N. Cahn, Rev. Mod. Phys. **57**, 563 (1985).
[37] S. Klimenko *et al.*, Fermilab Report No. FERMILAB-FN-0741, 2003.
[38] B. Ashmanskas *et al.*, Nucl. Instrum. Methods Phys. Res., Sect. A **518**, 532 (2004).
[39] D. J. Lange, Nucl. Instrum. Methods Phys. Res., Sect. A **462**, 152 (2001). We use version V00-14-05 downloaded from http://www.slac.stanford.edu/BFROOT/dist/packages/EvtGen/.
[40] R. Brun *et al.*, CERN Report No. CERN-DD-78-2-REV; CERN Programming Library Long Write-up W5013, 1993.
[41] F. James and M. Roos, Comput. Phys. Commun. **10**, 343 (1975).
[42] H. Plothow-Besch, PDFLIB: Nucleon, Pion and Photon Parton Density Function and α_s Calculations, User's Manual v. 6.06, PDFLIB Report No. W5051, CERN-PPE Report No. 1995.03.15.
[43] T. Affolder *et al.*, Phys. Rev. D **64**, 032002 (2001).
[44] The *BABAR* collaboration, https://oraweb.slac.stanford.edu/pls/slacquery/BABAR_DOCUMENTS.DetailedIndex?P_BP_ID=3553 (unpublished).
[45] M. Pivk and F. R. Le Diberder, Nucl. Instrum. Methods Phys. Res., Sect. A **555**, 356 (2005).
[46] W.-M. Yao *et al.*, J. Phys. G **33**, 1 (2006).
[47] D. Acosta *et al.*, Phys. Rev. D **71**, 032001 (2005).
[48] A. Abulencia *et al.*, Phys. Rev. Lett. **95**, 221805 (2005).
[49] The ALEPH Collaboration *et al.*, Phys. Rep. **427**, 257 (2006).
[50] M. Baarmand and F. Page (private communication).
[51] M. Cacciari (private communication).
[52] M. Cacciari *et al.*, Phys. Rev. D **55**, 7134 (1997).
[53] http://hepwww.rl.ac.uk/theory/seymour/herwig/HWtune.html.
[54] R. Seuster *et al.*, Phys. Rev. D **73**, 032002 (2006).
[55] M. Artuso *et al.*, Phys. Rev. D **70**, 112001 (2004).
[56] A. Atkas *et al.*, Eur. Phys. J. C **38**, 447 (2005).
[57] L. Gladilin, arXiv:hep-ex/9912064.
[58] L. K. Gladilin, arXiv:hep-ex/0607036.
[59] G. Abbiendi *et al.*, Eur. Phys. J. C **29**, 463 (2003).
[60] A. Heister *et al.*, Phys. Lett. B **512**, 30 (2001).
[61] K. Abe *et al.*, Phys. Rev. D **65**, 092006 (2002).
[62] R. Barate *et al.*, Eur. Phys. J. C **16**, 597 (2000).
[63] G. Corcella *et al.*, Proc. Sci. TOP2006 (2006) 035 [arXiv:hep-ph/0602191].